

000 001 002 003 004 005 006 007 008 009 010 011 012 013 014 015 016 017 018 019 020 021 022 023 024 025 026 027 028 029 030 031 032 033 034 035 036 037 038 039 040 041 042 043 044 045 046 047 048 049 050 051 052 053 LEARNING BETTER CERTIFIED MODELS FROM EMPIRICALLY-ROBUST TEACHERS

Anonymous authors

Paper under double-blind review

ABSTRACT

Adversarial training attains strong empirical robustness to specific adversarial attacks by training on concrete adversarial perturbations, but it produces neural networks that are not amenable to strong robustness certificates through neural network verification. On the other hand, earlier certified training schemes directly train on bounds from network relaxations to obtain models that are certifiably robust, but display sub-par standard performance. Recent work has shown that state-of-the-art trade-offs between certified robustness and standard performance can be obtained through a family of losses combining adversarial outputs and neural network bounds. Nevertheless, differently from empirical robustness, verifiability still comes at a significant cost in standard performance. In this work, we propose to leverage empirically-robust teachers to improve the performance of certifiably-robust models through knowledge distillation. Using a versatile feature-space distillation objective, we show that distillation from adversarially-trained teachers consistently improves on the state-of-the-art in certified training for ReLU networks across a series of robust computer vision benchmarks.

1 INTRODUCTION

Deep learning systems deployed in safety-critical applications must be robust to adversarial examples (Biggio et al., 2013; Szegedy et al., 2014; Goodfellow et al., 2015): imperceptible input perturbations that induce unintended behaviors such as misclassifications. Formal robustness certificates can be obtained through neural network verification algorithms (Tjeng et al., 2019; Lomuscio & Maganti, 2017; Ehlers, 2017). However, these techniques have a worst-case runtime that is exponential in network size even on piecewise-linear models (Katz et al., 2017). While *empirical* robustness to specific adversarial attacks can be attained by training against adversarial inputs (Madry et al., 2018), a technique known as adversarial training, neural network verifiers fail to provide robustness certificates on the resulting networks in a reasonable time. This is in spite of sustained progress in verification algorithms, which now couple specialized network convex relaxations (Zhang et al., 2018; Xu et al., 2021; Wong & Kolter, 2018; De Palma et al., 2024a) with efficient divide and conquer strategies (Bunel et al., 2020b; Henriksen & Lomuscio, 2021) within hardware-accelerated branch-and-bound frameworks (Wang et al., 2021; Ferrari et al., 2022; De Palma et al., 2021).

Networks amenable to robustness certificates through neural network verification can be obtained using so-called certified training schemes. Earlier approaches (Wong & Kolter, 2018; Zhang et al., 2020; Gowal et al., 2019; Mirman et al., 2018) proposed to train networks by computing the loss on neural network bounds obtained from convex relaxations, effectively deploying a building block of network verifiers within the training loop. Counter-intuitively, and owing to their relative smoothness and continuity, the loosest relaxations were found to outperform the others in this context (Jovanović et al., 2022; Lee et al., 2021). While the resulting networks enjoy strong verifiability using the same relaxations employed at training time, this is achieved at a significant cost in standard performance. Relying on branch-and-bound frameworks to perform post-training verification, a more recent line of works has shown that better trade-offs between certified robustness and standard performance can be obtained by combining methods based on convex relaxations with adversarial training (Balunovic & Vechev, 2020; De Palma et al., 2022; Müller et al., 2023; Mao et al., 2023). This was then formalized into the notion of *expressivity* (De Palma et al., 2024b), which entails the ability of a certified training loss to span a continuous range of trade-offs between pure adversarial training and the earlier losses based on convex relaxations, and can be easily implemented through convex combinations.

While, as attested by a recent study (Mao et al., 2025), networks trained through expressive losses produce state-of-the-art certifiably-robust models, their standard performance is still far from ideal. Noting that empirically-robust models display significantly better standard performance than certifiably-robust models (Croce et al., 2021), we believe they could be directly employed to improve the certified training process. Specifically, we aim to produce better certifiably-robust models by performing knowledge distillation (Hinton et al., 2015; Romero et al., 2015) from an empirically-robust teacher to the target model, leading to the following contributions:

- We introduce a novel and versatile feature-space distillation loss, which can transfer the knowledge of a teacher onto any convex combination between adversarial student features and bounds from its convex relaxations (§3.2).
- We tightly couple the proposed distillation objective with an existing expressive certified training loss, calling the CC-Dist the resulting algorithm (§3.3). We show that CC-Dist can successfully learn from an adversarially-trained teacher while at the same time significantly surpassing it in terms of certified robustness (§5.2).
- We present a comprehensive experimental evaluation of CC-Dist across medium and larger-scale vision benchmarks from the certified training literature, and show that the novel distillation loss enhances both standard performance and certified robustness across all considered benchmarks (§5.1). In particular, CC-Dist attains a new state-of-the-art for ReLU architectures on all setups, with significant improvements upon results from the literature on TinyImageNet and downscaled Imagenet.

We believe our work to be a further step towards bridging the ever-present gap between certified and empirical adversarial robustness. Code for CC-Dist is provided as part of the supplementary material.

2 BACKGROUND

Let lowercase letters denote scalars (e.g., $a \in \mathbb{R}$) boldface lowercase letters denote vectors (e.g., $\mathbf{a} \in \mathbb{R}^n$), uppercase letters denote matrices (e.g., $A \in \mathbb{R}^{n \times m}$), calligraphic letters denote sets (e.g. $\mathcal{A} \subset \mathbb{R}^n$) and brackets denote intervals (e.g., $[a, b]$). Furthermore, let lowercase single-letter subscripts denote vector indices (for instance, \mathbf{a}_i , or $f(\mathbf{a})_i$ for a vector-valued function f), and let the vector of all entries of \mathbf{a} except its i -th entry be denoted by $\mathbf{a}_{\bar{i}}$. We will write $\mathbf{1}^n \in \mathbb{R}^n$ for the unit vector, $I^n \in \mathbb{R}^{n \times n}$ for the identity matrix, and $_j I^n \in \mathbb{R}^{n \times n}$ for a matrix whose j -th column is the unit vector and filled with zeros otherwise. Abusing notation, given a vector-valued objective function $a(\mathbf{x})$ we will denote by $\min_{\mathbf{x} \in \mathcal{A}} a(\mathbf{x})$ the vector storing the minimum of $\min_{\mathbf{x} \in \mathcal{A}} a(\mathbf{x})_i$ in its i -th entry. Finally, we use the following shorthands: $[A]_+ := \max\{0, A\}$, $[A]_- := \min\{0, A\}$, $[\![a, b]\!] := \{a, a + 1, \dots, b\}$. [Appendix F](#) provides further details on the employed notation.

Let $(\mathbf{x}, y) \sim \mathcal{D}$ be a k -way classification dataset with points $\mathbf{x} \in \mathbb{R}^d$ and labels $y \in [\![1, k]\!]$. We aim to train a feed-forward ReLU neural network $f_\theta : \mathbb{R}^d \rightarrow \mathbb{R}^k$ with parameters $\theta \in \mathbb{R}^p$ such that each point \mathbf{x} from \mathcal{D} and the allowed adversarial perturbations $\mathcal{C}_\epsilon(\mathbf{x}) := \{\mathbf{x}' : \|\mathbf{x}' - \mathbf{x}\|_\infty \leq \epsilon\}$ around it are correctly classified:

$$\mathbf{x}' \in \mathcal{C}_\epsilon(\mathbf{x}) \implies \operatorname{argmax}_i f_\theta(\mathbf{x})_i = y. \quad (1)$$

2.1 NEURAL NETWORK VERIFICATION

Neural network verification is used to check whether equation (1) holds on a given network f_θ , providing a deterministic robustness certificate. Let $\mathbf{z}_{f_\theta}(\mathbf{x}, y)$ denote the differences between the ground truth logits and the other logits: $\mathbf{z}_{f_\theta}(\mathbf{x}, y) := (f_\theta(\mathbf{x})_y \mathbf{1}^k - f_\theta(\mathbf{x}))$. Verifiers solve the following optimization problem:

$$\mathbf{z}_{f_\theta}^{\mathcal{C}_\epsilon}(\mathbf{x}, y) := \min_{\mathbf{x}' \in \mathcal{C}_\epsilon(\mathbf{x})} \mathbf{z}_{f_\theta}(\mathbf{x}', y). \quad (2)$$

If all entries of $\mathbf{z}_{f_\theta}^{\mathcal{C}_\epsilon}(\mathbf{x}, y)$ are positive, then equation (1) holds, implying that the network is guaranteed to be robust to any given attack in $\mathcal{C}_\epsilon(\mathbf{x})$. An algorithm computing $\mathbf{z}_{f_\theta}^{\mathcal{C}_\epsilon}(\mathbf{x}, y)$ exactly is called a complete verifier: this is typically done through branch-and-bound (Bunel et al., 2018; De Palma et al., 2024a; Wang et al., 2021; Ferrari et al., 2022; Henriksen & Lomuscio, 2021). As this was shown to be NP-complete (Katz et al., 2017), a series of algorithms propose to compute

less expensive lower bounds $\mathbf{z}_{f_\theta}^{\mathcal{C}_\epsilon}(\mathbf{x}, y) \leq \mathbf{z}_{f_\theta}^{\mathcal{C}_\epsilon}(\mathbf{x}, y)$ (Zhang et al., 2018; Wong & Kolter, 2018; Dvijotham et al., 2018; Singh et al., 2019) by operating on network relaxations (incomplete verifiers), with $\mathbf{z}_{f_\theta}^{\mathcal{C}_\epsilon}(\mathbf{x}, y)_{\bar{y}} > 0$ successfully providing a robustness certificate. The least expensive incomplete verifier is called Interval Bound Propagation (IBP) (Gowal et al., 2019; Mirman et al., 2018), which is obtained by applying interval arithmetics (Sunaga, 1958; Hickey et al., 2001) to the network operators. We refer the reader to appendix A for further details.

2.2 CERTIFIED TRAINING

In principle, a network can be trained for verified robustness (certified training) by replacing the employed classification loss $\mathcal{L} : \mathbb{R}^k \times \llbracket 1, k \rrbracket \rightarrow \mathbb{R}$ (e.g., cross-entropy) with its worst-case across the adversarial perturbations (Madry et al., 2018):

$$\mathcal{L}_{f_\theta}^{\mathcal{C}_\epsilon}(\mathbf{x}, y) := \max_{\mathbf{x}' \in \mathcal{C}_\epsilon(\mathbf{x})} \mathcal{L}(f_\theta(\mathbf{x}'), y). \quad (3)$$

However, computing $\mathcal{L}_{f_\theta}^{\mathcal{C}_\epsilon}(\mathbf{x}, y)$ exactly is as hard as solving problem (2), and is hence typically replaced by an approximation. Let \mathbf{x}_{adv} denote the output of an adversarial attack, for instance PGD (Madry et al., 2018), on the network f_θ . Lower bounds to $\mathcal{L}_{f_\theta}^{\mathcal{C}_\epsilon}(\mathbf{x}, y)$ can be obtained by evaluating the loss at \mathbf{x}_{adv} :

$$\mathcal{L}_{f_\theta}^{\mathcal{C}_\epsilon}(\mathbf{x}, y) := \mathcal{L}(f_\theta(\mathbf{x}_{\text{adv}}), y) \leq \mathcal{L}_{f_\theta}^{\mathcal{C}_\epsilon}(\mathbf{x}, y). \quad (4)$$

Networks trained using $\mathcal{L}(f_\theta(\mathbf{x}_{\text{adv}}), y)$ (adversarial training) typically enjoy strong empirical robustness to the same types of attacks employed during training, but are not amenable to formal guarantees, which are the focus of this work. Assume the loss is monotonically increasing with respect to the non-ground-truth network logits and that it is translation-invariant: $\mathcal{L}(-\mathbf{z}_{f_\theta}(\mathbf{x}, y), y) = \mathcal{L}(f_\theta(\mathbf{x}), y)$ (Wong & Kolter, 2018). This holds for common losses such as cross-entropy. Given bounds $\mathbf{z}_{f_\theta}^{\mathcal{C}_\epsilon}(\mathbf{x}, y)$ from an incomplete verifier, and setting $\mathbf{z}_{f_\theta}^{\mathcal{C}_\epsilon}(\mathbf{x}, y)_y = 0$, an upper bound to $\mathcal{L}_{f_\theta}^{\mathcal{C}_\epsilon}(\mathbf{x}, y)$ can then be obtained as:

$$\mathcal{L}_{f_\theta}^{\mathcal{C}_\epsilon}(\mathbf{x}, y) := \mathcal{L}(-\mathbf{z}_{f_\theta}^{\mathcal{C}_\epsilon}(\mathbf{x}, y), y) \geq \mathcal{L}_{f_\theta}^{\mathcal{C}_\epsilon}(\mathbf{x}, y). \quad (5)$$

While networks trained via $\mathcal{L}(-\mathbf{z}_{f_\theta}^{\mathcal{C}_\epsilon}(\mathbf{x}, y), y)$ display strong verifiability through the same incomplete verifiers used to compute the $\mathbf{z}_{f_\theta}^{\mathcal{C}_\epsilon}(\mathbf{x}, y)$ bounds, the most successful option being IBP (Jovanović et al., 2022), they display sub-par standard performance. More recent and successful methods rely on losses featuring a combination between adversarial attacks and bounds from incomplete verifiers (De Palma et al., 2022; Balunovic & Vechev, 2020; Mao et al., 2023; Müller et al., 2023), pairing better standard performance with stronger verifiability through branch-and-bound. In particular, the ability of a loss function to span a continuous range of trade-offs between lower and upper bounds to $\mathcal{L}_{f_\theta}^{\mathcal{C}_\epsilon}(\mathbf{x}, y)$, termed *expressivity*, was found to be crucial to maximize performance (De Palma et al., 2024b). Nevertheless, the best-performing certifiably-robust models still display worse robustness-accuracy trade-offs than empirically-robust models (De Palma et al., 2024b; Croce et al., 2021).

2.3 KNOWLEDGE DISTILLATION

Knowledge distillation (Hinton et al., 2015) was introduced as a method to transfer the predictive ability of a large teacher model $t_{\theta^t} : \mathbb{R}^d \rightarrow \mathbb{R}^k$ onto the target model f_θ , termed the student. Let $\text{KL}_T : \mathbb{R}^k \times \mathbb{R}^k \rightarrow \mathbb{R}$ denote a KL divergence incorporating a softmax operation with temperature T . In its standard form, knowledge distillation pairs the employed classification loss with a KL divergence term where the teacher logits, termed soft labels, act as target distribution:

$$\mathcal{L}_{f_\theta}^{\text{KD}}(\lambda; \mathbf{x}, y) := \mathcal{L}(f_\theta(\mathbf{x}), y) + T^2 \lambda \text{KL}_T(f_\theta(\mathbf{x}), t_{\theta^t}(\mathbf{x})). \quad (6)$$

In order to provide more granular teacher information to the student, a series of works perform knowledge distillation on the intermediate activations (Romero et al., 2015; Zagoruyko & Komodakis, 2017; Heo et al., 2019): this is referred to as feature-space distillation. Let us write both the teacher and the student as the composition of a classification head with a feature map: $t_{\theta^t} := g_{\theta_g^t} \circ h_{\theta_h^t}$ and $f_\theta := g_{\theta_g} \circ h_{\theta_h}$, respectively, where $\theta^t = [\theta_h^t, \theta_g^t]^T$ and $\theta = [\theta_h, \theta_g]^T$. In its simplest form,

when the feature spaces of the teacher and student share the same dimensionality w , feature-space distillation encourages similarity between teacher and student features through a squared ℓ_2 term:

$$\mathcal{L}_{f_\theta}^{\text{F-KD}}(\lambda; \mathbf{x}, y) := \mathcal{L}(f_\theta(\mathbf{x}), y) + \lambda \left\| h_{\theta_h}(\mathbf{x}) - h_{\theta_h^t}^t(\mathbf{x}) \right\|_2^2.$$

Both $\mathcal{L}_{f_\theta}^{\text{KD}}(\lambda; \mathbf{x}, y)$ and $\mathcal{L}_{f_\theta}^{\text{F-KD}}(\lambda; \mathbf{x}, y)$ were originally designed to transfer standard network performance from teacher to student, and do not take robustness into account. Recent works have therefore focused on designing specialized distillation schemes that transfer either empirical adversarial robustness (Goldblum et al., 2020; Zhu et al., 2022; Zi et al., 2021; Muhammad et al., 2021) or probabilistic certified robustness (Vaishnavi et al., 2022) from teacher to student. Aiming to improve state-of-the-art trade-offs between deterministic certified robustness and standard performance, we will present a novel training scheme that transfers knowledge from an empirically-robust teacher through feature-space distillation.

3 KNOWLEDGE DISTILLATION FOR CERTIFIED ROBUSTNESS

We aim to leverage the empirical robustness of adversarially-trained networks to train better certifiably-robust models. Owing to its state-of-the-art certified training performance, we will couple an existing expressive loss function (§3.1) with a novel and versatile feature-space distillation term (§3.2). Pseudo-code and proofs of technical results are respectively provided in appendices C and B.

3.1 EXPRESSIVE LOSSES: CC-IBP

De Palma et al. (2024b) define a parametrized loss function $\mathcal{L}_{f_\theta}^{\mathcal{C}_\epsilon}(\alpha; \mathbf{x}, y)$ to be expressive if: (i) $\mathcal{L}_{f_\theta}^{\mathcal{C}_\epsilon}(0; \mathbf{x}, y) = \mathcal{L}_{f_\theta}^{\mathcal{C}_\epsilon}(\mathbf{x}, y)$ and $\mathcal{L}_{f_\theta}^{\mathcal{C}_\epsilon}(1; \mathbf{x}, y) = \bar{\mathcal{L}}_{f_\theta}^{\mathcal{C}_\epsilon}(\mathbf{x}, y)$; (ii) $\mathcal{L}_{f_\theta}^{\mathcal{C}_\epsilon}(\mathbf{x}, y) \leq \mathcal{L}_{f_\theta}^{\mathcal{C}_\epsilon}(\alpha; \mathbf{x}, y) \leq \bar{\mathcal{L}}_{f_\theta}^{\mathcal{C}_\epsilon}(\mathbf{x}, y)$ $\forall \alpha \in [0, 1]$; (iii) $\mathcal{L}_{f_\theta}^{\mathcal{C}_\epsilon}(\alpha; \mathbf{x}, y)$ is continuous and monotonically increasing for $\alpha \in [0, 1]$.

As demonstrated by the empirical performance of three different expressive losses obtained through convex combinations between adversarial and incomplete verification terms, expressivity results in state-of-the-art certified training performance (De Palma et al., 2024b). We here focus on CC-IBP, which implements an expressive loss by evaluating \mathcal{L} on convex combinations between adversarial logit differences $\mathbf{z}_{f_\theta}(\mathbf{x}_{\text{adv}})$ and lower bounds $\underline{\mathbf{z}}_{f_\theta}^{\mathcal{C}_\epsilon}(\mathbf{x}, y)$ to the logit differences computed via IBP:

$$\begin{aligned} \text{CC } \mathcal{L}_{f_\theta}^{\mathcal{C}_\epsilon}(\alpha; \mathbf{x}, y) &:= \mathcal{L}\left(-\text{CC } \mathbf{z}_{f_\theta}^{\mathcal{C}_\epsilon}(\alpha; \mathbf{x}, y), y\right), \\ \text{where: } \text{CC } \mathbf{z}_{f_\theta}^{\mathcal{C}_\epsilon}(\alpha; \mathbf{x}, y) &:= (1 - \alpha) \mathbf{z}_{f_\theta}(\mathbf{x}_{\text{adv}}, y) + \alpha \underline{\mathbf{z}}_{f_\theta}^{\mathcal{C}_\epsilon}(\mathbf{x}, y). \end{aligned} \quad (7)$$

As we will show in §3.3, CC-IBP can be tightly coupled with a specialized distillation loss, which we present in the next subsection.

3.2 DISTILLATION LOSS

Certified training is concerned with worst-case network behavior. Mirroring the robust loss in §2.2, a worst-case feature-space distillation loss over the perturbations would take the following form:

$$\mathcal{R}_{f_\theta}^{\mathcal{C}_\epsilon}(\mathbf{x}, y) := \max_{\mathbf{x}' \in \mathcal{C}_\epsilon(\mathbf{x})} \left\| h_{\theta_h}(\mathbf{x}') - h_{\theta_h^t}^t(\mathbf{x}) \right\|_2^2. \quad (8)$$

However, as for $\mathcal{L}_{f_\theta}^{\mathcal{C}_\epsilon}(\mathbf{x}, y)$, computing $\mathcal{R}_{f_\theta}^{\mathcal{C}_\epsilon}(\mathbf{x}, y)$ exactly amounts to solving a non-convex optimization problem over the features. As for equation (4), a lower bound $\underline{\mathcal{R}}_{f_\theta}^{\mathcal{C}_\epsilon}(\mathbf{x}, y)$ can be obtained by evaluating the left-hand side of equation (8) at the adversarial input \mathbf{x}_{adv} :

$$\mathcal{R}_{f_\theta}^{\mathcal{C}_\epsilon}(\mathbf{x}, y) := \left\| h_{\theta_h}(\mathbf{x}_{\text{adv}}) - h_{\theta_h^t}^t(\mathbf{x}) \right\|_2^2 \leq \mathcal{R}_{f_\theta}^{\mathcal{C}_\epsilon}(\mathbf{x}, y).$$

Similarly to $\bar{\mathcal{L}}_{f_\theta}^{\mathcal{C}_\epsilon}(\mathbf{x}, y)$, an upper bound $\bar{\mathcal{R}}_{f_\theta}^{\mathcal{C}_\epsilon}(\mathbf{x}, y)$ can be instead computed resorting to IBP.

Proposition 3.1. *Let $h_{\theta_h}^{\mathcal{C}_\epsilon}(\mathbf{x})$ and $\bar{h}_{\theta_h}^{\mathcal{C}_\epsilon}(\mathbf{x})$ respectively denote IBP lower and upper bounds to the student features:*

$$h_{\theta_h}^{\mathcal{C}_\epsilon}(\mathbf{x}) \leq h_{\theta_h}(\mathbf{x}') \leq \bar{h}_{\theta_h}^{\mathcal{C}_\epsilon}(\mathbf{x}), \quad \forall \mathbf{x}' \in \mathcal{C}_\epsilon(\mathbf{x}).$$

216 The loss function $\bar{\mathcal{R}}_{f_\theta}^{\mathcal{C}_\epsilon}(\mathbf{x}, y) := \sum_i \max \left\{ \left(\underline{h}_{\theta_h}^{\mathcal{C}_\epsilon}(\mathbf{x})_i - h_{\theta_h^t}^t(\mathbf{x})_i \right)^2, \left(\bar{h}_{\theta_h}^{\mathcal{C}_\epsilon}(\mathbf{x})_i - h_{\theta_h^t}^t(\mathbf{x})_i \right)^2 \right\}$ is an
 217 upper bound to the worst-case distillation loss from equation (8): $\bar{\mathcal{R}}_{f_\theta}^{\mathcal{C}_\epsilon}(\mathbf{x}, y) \geq \mathcal{R}_{f_\theta}^{\mathcal{C}_\epsilon}(\mathbf{x}, y)$.
 218
 219

220 In order to preserve the greatest degree of flexibility, and mirroring expressive losses (§3.1), we aim to
 221 design a parametrized feature-space distillation loss ${}^{CC}\mathcal{R}_{f_\theta}^{\mathcal{C}_\epsilon}(\alpha; \mathbf{x}, y)$ that can span a continuous range
 222 of trade-offs between $\mathcal{R}_{f_\theta}^{\mathcal{C}_\epsilon}(\mathbf{x}, y)$ and $\bar{\mathcal{R}}_{f_\theta}^{\mathcal{C}_\epsilon}(\mathbf{x}, y)$. Let us denote by ${}^{CC}\bar{h}_{\theta_h}^{\mathcal{C}_\epsilon}(\alpha; \mathbf{x})$ and ${}^{CC}\underline{h}_{\theta_h}^{\mathcal{C}_\epsilon}(\alpha; \mathbf{x})$ con-
 223 vex combinations of the adversarial student features $h_{\theta_h}(\mathbf{x}_{\text{adv}})$ with $\bar{h}_{\theta_h}^{\mathcal{C}_\epsilon}(\mathbf{x})$ and $\underline{h}_{\theta_h}^{\mathcal{C}_\epsilon}(\mathbf{x})$, respectively:
 224

$$\begin{aligned} {}^{CC}\bar{h}_{\theta_h}^{\mathcal{C}_\epsilon}(\alpha; \mathbf{x}) &:= (1 - \alpha) h_{\theta_h}(\mathbf{x}_{\text{adv}}) + \alpha \bar{h}_{\theta_h}^{\mathcal{C}_\epsilon}(\mathbf{x}), \\ {}^{CC}\underline{h}_{\theta_h}^{\mathcal{C}_\epsilon}(\alpha; \mathbf{x}) &:= (1 - \alpha) h_{\theta_h}(\mathbf{x}_{\text{adv}}) + \alpha \underline{h}_{\theta_h}^{\mathcal{C}_\epsilon}(\mathbf{x}). \end{aligned} \quad (9)$$

225 As we next show, ${}^{CC}\mathcal{R}_{f_\theta}^{\mathcal{C}_\epsilon}(\alpha; \mathbf{x}, y)$ can be realized by distilling onto ${}^{CC}\bar{h}_{\theta_h}^{\mathcal{C}_\epsilon}(\alpha; \mathbf{x})$ and ${}^{CC}\underline{h}_{\theta_h}^{\mathcal{C}_\epsilon}(\alpha; \mathbf{x})$.
 226
 227

228 **Proposition 3.2.** *The loss function*

$${}^{CC}\mathcal{R}_{f_\theta}^{\mathcal{C}_\epsilon}(\alpha; \mathbf{x}, y) := \sum_i \max \left\{ \left({}^{CC}\underline{h}_{\theta_h}^{\mathcal{C}_\epsilon}(\alpha; \mathbf{x})_i - h_{\theta_h^t}^t(\mathbf{x})_i \right)^2, \left({}^{CC}\bar{h}_{\theta_h}^{\mathcal{C}_\epsilon}(\alpha; \mathbf{x})_i - h_{\theta_h^t}^t(\mathbf{x})_i \right)^2 \right\}$$

229 enjoys the following properties:
 230
 231

- 232 1. ${}^{CC}\mathcal{R}_{f_\theta}^{\mathcal{C}_\epsilon}(0; \mathbf{x}, y) = \mathcal{R}_{f_\theta}^{\mathcal{C}_\epsilon}(\mathbf{x}, y)$ and ${}^{CC}\mathcal{R}_{f_\theta}^{\mathcal{C}_\epsilon}(1; \mathbf{x}, y) = \bar{\mathcal{R}}_{f_\theta}^{\mathcal{C}_\epsilon}(\mathbf{x}, y)$;
- 233 2. $\mathcal{R}_{f_\theta}^{\mathcal{C}_\epsilon}(\mathbf{x}, y) \leq {}^{CC}\mathcal{R}_{f_\theta}^{\mathcal{C}_\epsilon}(\alpha; \mathbf{x}, y) \leq \bar{\mathcal{R}}_{f_\theta}^{\mathcal{C}_\epsilon}(\mathbf{x}, y) \forall \alpha \in [0, 1]$;
- 234 3. ${}^{CC}\mathcal{R}_{f_\theta}^{\mathcal{C}_\epsilon}(\alpha; \mathbf{x}, y)$ is continuous and monotonically increasing for $\alpha \in [0, 1]$.

235 3.3 CC-DIST

236 While we expect special cases ${}^{CC}\mathcal{R}_{f_\theta}^{\mathcal{C}_\epsilon}(0; \mathbf{x}, y)$ and ${}^{CC}\mathcal{R}_{f_\theta}^{\mathcal{C}_\epsilon}(1; \mathbf{x}, y)$ to work well on settings where
 237 CC-IBP is employed with small or large α values, respectively, we aim to leverage the full flexibility
 238 from proposition 3.2 to obtain consistent performance across setups.
 239

240 We will now show that, if the student uses an affine classification head, the CC-IBP convex com-
 241 binations ${}^{CC}\mathbf{z}_{f_\theta}^{\mathcal{C}_\epsilon}(\alpha; \mathbf{x}, y)$ correspond to a simple affine function of ${}^{CC}\underline{h}_{\theta_h}^{\mathcal{C}_\epsilon}(\alpha; \mathbf{x})$ and ${}^{CC}\bar{h}_{\theta_h}^{\mathcal{C}_\epsilon}(\alpha; \mathbf{x})$,
 242 onto which distillation is performed. Consequently, we propose to employ the same α parameter for
 243 both ${}^{CC}\mathcal{R}_{f_\theta}^{\mathcal{C}_\epsilon}(\alpha; \mathbf{x}, y)$ and ${}^{CC}\mathcal{L}_{f_\theta}^{\mathcal{C}_\epsilon}(\alpha; \mathbf{x}, y)$, thus tightly coupling our distillation loss with CC-IBP.
 244

245 **Lemma 3.3.** *Let the student classification head $g_{\theta_g}(\mathbf{a})$ be affine, and let $\tilde{g}_{\theta_g}^y(\mathbf{a}) := \tilde{W}^n \mathbf{a} + \tilde{\mathbf{b}}^n$ be
 246 its composition with the operator performing the difference between logits. We can write the CC-IBP
 247 convex combinations as:*

$${}^{CC}\mathbf{z}_{f_\theta}^{\mathcal{C}_\epsilon}(\alpha; \mathbf{x}, y) = \begin{bmatrix} [\tilde{W}^n]_+ & [\tilde{W}^n]_- \end{bmatrix} \begin{bmatrix} {}^{CC}\underline{h}_{\theta_h}^{\mathcal{C}_\epsilon}(\alpha; \mathbf{x}) \\ {}^{CC}\bar{h}_{\theta_h}^{\mathcal{C}_\epsilon}(\alpha; \mathbf{x}) \end{bmatrix} + \tilde{\mathbf{b}}^n.$$

248 **CC-Dist loss** Let β be the distillation coefficient, determining the relative weight of the distillation
 249 term. Omitting any regularization, the overall training loss for CC-Dist (short for CC-IBP Distillation)
 250 takes the following form:
 251

$$\mathcal{L}^{\text{CC-Dist}}(\alpha, \beta; \mathbf{x}, y) := {}^{CC}\mathcal{L}_{f_\theta}^{\mathcal{C}_\epsilon}(\alpha; \mathbf{x}, y) + \beta {}^{CC}\mathcal{R}_{f_\theta}^{\mathcal{C}_\epsilon}(\alpha; \mathbf{x}, y). \quad (10)$$

252 In practice, denoting by w the dimensionality of the feature space, unless stated otherwise, we employ
 253 $\beta = 5/w$ in all reported experiments owing to its consistent performance across setups.
 254

255 **Teacher models** We propose to use teacher models trained via pure adversarial training (see §2.2)
 256 on the target task, employing the same architecture as the student. In order to comply with the
 257 conditions of lemma 3.3, we define the features as the activations before the last affine network layer.
 258

270 **Intuition** We expect teachers to transfer part of their superior natural accuracy and empirical
 271 robustness to the target models. While the teacher certified robustness will be significantly smaller
 272 than for models trained via certified training, the CC-IBP term in equation (10) is employed to
 273 preserve student verifiability, hence increasing its certified robustness. Experimental evidence is
 274 provided in §5.2 and appendix E.1.

276 4 RELATED WORK

277 Owing to its favorable optimization properties (Jovanović et al., 2022), the relatively loose IBP
 278 (§2.1) is the method of choice (Mao et al., 2024a) when computing lower bounds to equation (2)
 279 to be employed for certified training. Tighter techniques are however preferred within branch-
 280 and-bound-based complete verifiers. Branch-and-bound (Bunel et al., 2018) couples a bounding
 281 algorithm with a strategy to refine the network relaxations by iteratively splitting problem (2) into
 282 subproblems (branching), which typically operates by splitting piecewise linearities into their linear
 283 components (De Palma et al., 2021; Henriksen & Lomuscio, 2021; Ferrari et al., 2022; Bunel
 284 et al., 2020b). Earlier bounding algorithms relied on linear network relaxations (Bunel et al.,
 285 2018; Ehlers, 2017; Anderson et al., 2020), with more effective techniques operating in the dual
 286 space (Dvijotham et al., 2018; Bunel et al., 2020a; De Palma et al., 2024a). State-of-the-art branch-
 287 and-bound frameworks have since converged to using fast bounds based on propagating couples
 288 of linear bounds through the network (Zhang et al., 2018; Singh et al., 2019; Xu et al., 2021) with
 289 Lagrangian relaxations employed to capture additional constraints (Wang et al., 2021; Ferrari et al.,
 290 2022; Zhang et al., 2022c; Zhou et al., 2024).

291 Earlier certified training works add geometric regularizers to the standard adversarial training
 292 loss (Xiao et al., 2019; Croce et al., 2019; Liu et al., 2021). Recent certified training schemes mix
 293 adversarial training with bounds from network relaxations to obtain strong post-training verifiability
 294 using branch-and-bound (see §2.2). Balunovic & Vechev (2020) perform adversarial attacks over
 295 latent-space over-approximations. The good performance of the latter at lower perturbation radii
 296 was matched through a regularizer on the area of network relaxations (De Palma et al., 2022),
 297 IBP-R, and later refined by connecting the gradients of the over-approximation with those of the
 298 attack (TAPS) (Mao et al., 2023). Another work, named SABR, proposed to compute network
 299 relaxations over a subset of \mathcal{C}_ϵ and to tune the subset size for each benchmark. This was then
 300 generalized into the notion of expressive losses (De Palma et al., 2024b) (see §3.1), which includes
 301 losses based on convex combinations forming the basis of this work. All the above methods train
 302 standard feedforward ReLU networks using convex relaxations, with IBP bounds being the most
 303 prevalent among them. Recent work has highlighted the superior representational power of networks
 304 trained via tighter relaxations (Baader et al., 2024; Mao et al., 2024b), and sought to overcome the
 305 associated optimization challenges (Balauca et al., 2025). Certifiably-robust networks can also be
 306 obtained by training 1-Lipschitz models using alternative architectures (Zhang et al., 2021; 2022a),
 307 the best-performing being SortNet (Zhang et al., 2022b). These were also shown to benefit from
 308 additional generated data (Altstidl et al., 2024), whose use is beyond the focus of our work. While we
 309 here concentrate on ℓ_∞ perturbations and deterministic certificates, 1-Lipschitz architectures (Prach
 310 et al., 2024; Meunier et al., 2022) and Lipschitz regularization (Hu et al., 2023; Leino et al.) are
 311 very effective when \mathcal{C}_ϵ is defined using the ℓ_2 norm, setting under which probabilistic robustness
 312 certificates can be effectively obtained using randomised smoothing (Cohen et al., 2019).

313 Many specialized knowledge distillation schemes designed to transfer empirical robustness focus
 314 on modifying the logit-space distillation loss from equation (6). Assuming an adversarially-trained
 315 teacher, ARD (Goldblum et al., 2020) proposes to modify the KL term from equation (6) to evaluate
 316 the student on an adversarially-perturbed input. IAD (Zhu et al., 2022), instead, replaces the cross-
 317 entropy loss with a KL term between the student’s perturbed and unperturbed outputs, weighted
 318 according to the teacher’s inability to correctly classify the adversarial input. RSLAD (Zi et al., 2021)
 319 removes the dynamic weighting and trains with two KL terms between teacher and student: one
 320 using clean inputs, the other where the student is evaluated on a perturbation seeking to maximize the
 321 distance from the clean teacher output. In this context, less attention has been devoted to feature-space
 322 distillation methods (Muhammad et al., 2021). CRD (Vaishnavi et al., 2022) presented a logit-space
 323 distillation loss designed to transfer probabilistic certified robustness, relying on a sum of the student
 cross-entropy loss with an ℓ_2 term on the models softmax outputs, all evaluated on random Gaussian
 perturbations. The focus of all the above works is to transfer some of the performance of larger

and more capable models onto smaller and less expensive architectures. However, it was shown that training a network for a given task, and then re-using it to distill knowledge onto a second model with the same architecture and training goal can improve performance through regularization. This was observed both in the context of standard training (Furlanello et al., 2018), and of pure adversarial training for empirical robustness (Chen et al., 2020). Finally, closely-related works at the intersection between knowledge distillation and deterministic certified robustness include: (i) investigating how robustness guarantees obtained on a student can be transferred from a distilled student to its teacher (Indri et al., 2024), and (ii) distilling a non-robust perceptual similarity metric onto a 1-Lipschitz architecture to obtain a certifiably-robust perceptual similarity metric (Ghazanfari et al., 2024). In this work, targeting supervised classification tasks from the robust vision literature and using techniques based on convex relaxations, we aim to leverage an empirically-robust yet hard-to-verify teacher to improve the deterministic certified robustness of a student with the same architecture.

Table 1: Evaluation of the effect of CC-Dist compared to pure CC-IBP (De Palma et al., 2024b) when training for certified robustness against ℓ_∞ norm perturbations. Literature results are provided as a reference. We highlight in bold the entries corresponding to the largest standard or certified accuracy for each benchmark, and, when they do not coincide, underline the best accuracies for ReLU-based architectures.

	Dataset	ϵ	Method	Source	Standard acc. [%]	Certified acc. [%]
255	CIFAR-10	$\frac{2}{255}$	CC-DIST	this work	81.55	64.60
			CC-IBP	this work	79.51	63.50
			CC-IBP	De Palma et al. (2024b)	80.09	63.78
			MTL-IBP †	Mao et al. (2025)	78.82	64.41
			STAPS	Mao et al. (2023)	79.76	62.98
			SABR †	Mao et al. (2024a)	79.89	63.28
			SORTNET	Zhang et al. (2022b)	67.72	56.94
			IBP-R †	Mao et al. (2024a)	80.46	62.03
			IBP †	Mao et al. (2024a)	68.06	56.18
			CROWN-IBP †	Mao et al. (2025)	67.60	53.97
255	TinyImageNet	$\frac{8}{255}$	CC-DIST	this work	55.13	<u>35.52</u>
			CC-IBP	this work	54.46	35.42
			CC-IBP	De Palma et al. (2024b)	53.71	35.27
			MTL-IBP †	Mao et al. (2025)	54.28	35.41
			STAPS	Mao et al. (2023)	52.82	34.65
			SABR †	Mao et al. (2025)	52.71	35.34
			SORTNET	Zhang et al. (2022b)	54.84	40.39
			IBP-R	De Palma et al. (2022)	52.74	27.55
			IBP	Shi et al. (2021)	48.94	34.97
			CROWN-IBP †	Mao et al. (2025)	48.25	32.59
255	ImageNet64	$\frac{1}{255}$	CC-DIST	this work	43.78	27.88
			CC-IBP	this work	41.28	26.53
			EXP-IBP	De Palma et al. (2024b)	38.71	26.18
			MTL-IBP †	Mao et al. (2025)	35.97	27.73
			STAPS †	Mao et al. (2025)	30.63	22.31
			SABR †	De Palma et al. (2024b)	38.68	25.85
			SORTNET	Zhang et al. (2022b)	25.69	18.18
			IBP †	Mao et al. (2025)	26.77	19.82
			CROWN-IBP †	Mao et al. (2025)	28.44	22.14
			CC-DIST	this work	28.17	13.96
255	ImageNet64	$\frac{1}{255}$	CC-IBP	this work	25.94	13.69
			EXP-IBP	De Palma et al. (2024b)	22.73	13.30
			SABR †	De Palma et al. (2024b)	20.33	12.39
			SORTNET	Zhang et al. (2022b)	14.79	9.54
			CROWN-IBP	Xu et al. (2020)	16.23	8.73
			IBP	Gowal et al. (2019)	15.96	6.13

† Evaluation from later work attaining a larger standard or certified accuracy than reported in the original work.

378

5 EXPERIMENTAL EVALUATION

381 This section presents an experimental evaluation of the proposed distillation scheme, focusing on
 382 image classification datasets from the certified training literature. We first present results on the
 383 effectiveness of our novel distillation loss (§5.1), followed by a comparison of the trained models with
 384 their teachers (§5.2), and by an analysis of the effect of the distillation coefficient on CC-Dist (§5.3).

385 In line with previous work (Müller et al., 2023; Mao et al., 2023; Shi et al., 2021; De Palma et al.,
 386 2024b), all the models trained via CC-Dist in this evaluation are based a 7-layer convolutional archi-
 387 tecture named CNN-7, regularized using an ℓ_1 term. The teacher models are trained via adversarial
 388 training based on a 10-step PGD adversary (Madry et al., 2018) and ℓ_1 regularization. As this was
 389 found to be beneficial in practice, we employ the CNN-7 architecture for the teacher model too.
 390 We implemented CC-Dist in PyTorch (Paszke et al., 2019) similarly to the expressive losses code-
 391 base (De Palma et al., 2024b), also relying on `auto_LiRPA` (Xu et al., 2020) to compute IBP bounds.
 392 As common in the wider certified training literature (Müller et al., 2023; Mao et al., 2023), we employ
 393 the custom regularization and initialization introduced by Shi et al. (2021). Post-training verification
 394 is performed using the OVAL branch-and-bound framework (Bunel et al., 2018; 2020a; De Palma
 395 et al., 2021) similarly to De Palma et al. (2022; 2024b), using a configuration based on α - β -CROWN
 396 network bounds (Wang et al., 2021; Xu et al., 2021) and employing at most 600 seconds per image.
 397 Additional details and supplementary experiments can be found in appendices D and E, respectively.

400

5.1 CC-DIST EVALUATION

402 We now evaluate the performance of CC-Dist (§3.3) with respect to pure CC-IBP (De Palma et al.,
 403 2024b), and compare the resulting performance with results taken from the certified training literature.
 404 For each method from the literature, we report the best attained performance across previous works
 405 and network architectures. In order to isolate the effect of any modification within our codebase
 406 and experimental setup, we report both CC-IBP results from our evaluations, and the literature results
 407 corresponding to the best-performing expressive loss (CC-IBP, MTL-IBP, or Exp-IBP) from the
 408 original work (De Palma et al., 2024b). Table 1 shows that the distillation loss improves on both the
 409 standard and the certified accuracies of pure CC-IBP across all the considered CIFAR-10 (Krizhevsky
 410 & Hinton, 2009), TinyImageNet (Le & Yang, 2015), and downscaled ImageNet (64 \times 64) (Chrabaszcz
 411 et al., 2017) benchmarks. Consequently, CC-Dist establishes a new state-of-the-art, improving on
 412 both standard and certified accuracy compared to previously-reported results, on all benchmarks except
 413 CIFAR-10 with $\epsilon = 8/255$. Differently from the other settings, the best certified accuracy on this
 414 benchmark is attained by SortNet (Zhang et al., 2022b), which uses a specialized 1-Lipschitz network
 415 architecture (see §4). Its performance on this setup can be further improved through the use of addi-
 416 tional generated data (Altstidl et al., 2024), which is outside the scope of our work. While the sub-par
 417 performance of ReLU networks on this benchmark is well known in the literature (Müller et al., 2023;
 418 De Palma et al., 2024b), we are hopeful that distillation from empirically-robust teachers may be
 419 beneficial to 1-Lipschitz networks too, and defer the investigation to future work. On TinyImageNet
 420 and downscaled ImageNet we found that both the standard and certified accuracies of CC-IBP benefit
 421 from a smaller α coefficient than those employed in De Palma et al. (2024b), explaining the difference
 422 between our CC-IBP results and those reported in the original work. Owing to the combined effect of
 423 this and of the benefits of our novel distillation loss, the difference between CC-Dist and the results
 424 from the literature is particularly remarkable on these two larger-scale benchmarks.

425 Appendix E.1 sheds light on the success of our distillation technique by analyzing differences in
 426 empirical robustness and IBP regularization between CC-IBP and CC-Dist. Appendices E.2, E.3
 427 and E.8 demonstrate the wider potential of knowledge distillation for certified training by showing
 428 (i) the effectiveness of special cases of the proposed distillation loss, (ii) that SABR, **MTL-IBP**, and
 429 **IBP-R** benefit from a similar distillation process and (iii) that CC-Dist is effective on a different model
 430 architecture and activation function. Appendices E.4 and E.9 respectively investigate the performance
 431 of logit-based distillation, and of using earlier features for ${}^{CC}\mathcal{R}_{f_\theta}^{C_e}(\alpha; \mathbf{x}, y)$. Appendix E.10 shows
 432 that employing clean teachers results in worse performance profiles, highlighting the importance
 433 of robust representations.

Table 2: Comparison between the CC-Dist student models from table 1 and the respective teacher models.

Dataset	ϵ	Method	Standard acc. [%]	AA acc. [%]	Certified acc. \dagger [%]
CIFAR-10	$\frac{2}{255}$	STUDENT	81.55	70.71	64.4
		TEACHER	88.23	73.26	1.2
	$\frac{8}{255}$	STUDENT	55.13	36.80	35.8
		TEACHER	78.16	41.62	0.0
TinyImageNet	$\frac{1}{255}$	STUDENT	43.78	32.30	32.6
		TEACHER	47.18	34.17	17.4
ImageNet64	$\frac{1}{255}$	STUDENT	28.17	17.87	5.6
		TEACHER	40.30	25.34	0.0

\dagger Certified accuracy reported over the first 500 test images.

5.2 TEACHER-STUDENT COMPARISON

In order to provide insights on the distillation process, we now present a comparison of the performance of the CC-Dist models from table 1 with that of the respective teacher models. Owing to the extremely large computational cost associated to running branch-and-bound on networks trained via pure adversarial training (the teachers), we restrict the certified robustness comparison on the first 500 images of the test set of each benchmark. Table 2 shows a clear difference in terms of standard accuracy and empirical robustness to [AutoAttack](#) (Croce & Hein, 2020) between teacher and student, the latter displaying worse performance as expected. On the other hand, the teachers fail to attain good certified robustness across any of the considered benchmarks, highlighting that the students significantly surpass the respective teachers in terms of verifiability. In other words, the distillation process successfully exploits empirically-robust teachers to improve the state-of-the-art in certifiably-robust models.

5.3 SENSITIVITY TO DISTILLATION COEFFICIENT

We now present an empirical study of the effect of the distillation coefficient β on the performance profiles of CC-Dist. As mentioned in §3.3, we keep $\beta = 5/w$ throughout all the experiments, where w denotes the dimensionality of the feature space. This is in order to avoid the introduction of an additional hyper-parameter, and owing to its strong performance across the considered settings. Figure 1 compares the behavior at $\beta = 5/w$ from table 1, where both certified robustness via branch-and-bound and standard performance are enhanced, with results for different distillation coefficients. It reports standard performance, empirical adversarial robustness (measured through the attacks within the employed branch-and-bound framework), and certified robustness (both using branch-and-bound and the best results between incomplete verifiers CROWN (Zhang et al., 2018) and IBP (Gowal et al., 2019)) across β values on the CIFAR-10 test set. For $\epsilon = 2/255$, increasing β leads to a steady increase in both standard accuracy and empirical robustness. At the same time, verifiability increases until an intermediate β value, then steadily decreases, with the certified accuracy via incomplete verifiers peaking at a lower value than when using branch-and-bound. This

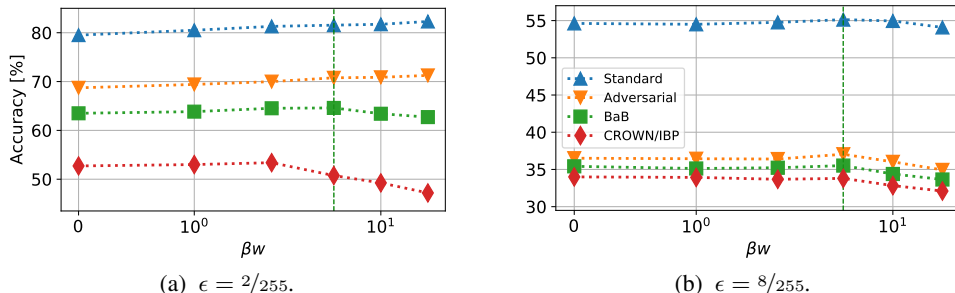


Figure 1: Standard, empirical adversarial and certified accuracies (BaB and CROWN/IBP) under ℓ_∞ perturbations of networks trained using CC-Dist under varying distillation coefficient β . The legend is reported once for all subfigures in plot 1(b). Metrics are reported on the CIFAR-10 test set. The β value employed throughout the paper (see §3.3) is marked by a dashed vertical line.

486 is similar to the behavior of the α parameter in expressive losses such as CC-IBP (De Palma et al.,
 487 2024b). As also visible in table 1, distillation appears to be less helpful for $\epsilon = 8/255$, where standard
 488 performance is enhanced only for intermediate β values. We explain this difference through the
 489 larger degree of similarity between teacher and student on $\epsilon = 2/255$: see table 2.
 490

491 6 CONCLUSIONS

492 We presented a novel training scheme, named CC-Dist, that successfully leverages empirically-robust
 493 models to train better certifiably-robust neural networks through knowledge distillation. Complementing
 494 CC-IBP, CC-Dist relies on a versatile feature-space distillation loss that can operate on convex
 495 combinations between bounds from student convex relaxations and adversarial student features. We
 496 show that CC-Dist improves on both the standard and certified robust accuracies of CC-IBP on all con-
 497 sidered benchmarks from the robust vision literature, in spite of the relatively low certified robustness
 498 of the employed teacher models. As a result, CC-Dist attains a new state-of-the-art in certified training
 499 across ReLU architectures, showcasing the potential of knowledge distillation for certified robustness.
 500 While our work focuses on teachers that employ the same architecture as the student, we are hopeful
 501 that further progress can be made by appropriately training teachers with larger effective capacity.
 502

503 ETHICS STATEMENT

504 We do not anticipate any short-term negative impact of certifiably-robust networks. Indeed, we
 505 believe that efficient certified training techniques should be primarily leveraged towards providing
 506 guarantees to deep learning systems operating in safety-critical contexts. Nevertheless, we acknowl-
 507 edge that adversarial attacks may have social utility when deployed against unethical systems, which
 508 constitute unintended use of machine learning technologies, pointing to a potential shortcoming of
 509 provable robustness. Effective mitigation strategies may include targeted regulations.
 510

513 REPRODUCIBILITY STATEMENT

514 Code for CC-Dist is provided as part of the supplementary material, and pseudo-code is provided in
 515 appendix C. Information to reproduce the experiments can be found in §5 and appendix D, which
 516 also includes details on the employed compute resources and software acknowledgments. Owing to
 517 the large cost associated with the verification experiments (a timeout of 600 seconds per evaluation
 518 image is employed), and complying with related previous works (De Palma et al., 2024b; Mao et al.,
 519 2023; Müller et al., 2023; Mao et al., 2024a; 2025), we provide single-seed results. An indication of
 520 experimental variability on a single dataset is nevertheless provided in appendix E.6.
 521

523 REFERENCES

524 Thomas Altstidl, David Dobre, Arthur Kosmala, Bjoern Eskofier, Gauthier Gidel, and Leo Schwinn.
 525 On the scalability of certified adversarial robustness with generated data. In *Advances in Neural*
 526 *Information Processing Systems*, 2024.

527 Ross Anderson, Joey Huchette, Will Ma, Christian Tjandraatmadja, and Juan Pablo Vielma. Strong
 528 mixed-integer programming formulations for trained neural networks. *Mathematical Programming*,
 529 2020.

530 Maksym Andriushchenko and Nicolas Flammarion. Understanding and improving fast adversarial
 531 training. In *Advances in Neural Information Processing Systems*, 2020.

532 Maximilian Baader, Mark Niklas Mueller, Yuhao Mao, and Martin Vechev. [Expressivity of ReLU-](#)
 533 [Networks under Convex Relaxations](#). In *International Conference on Learning Representations*,
 534 2024.

535 Stefan Balauca, Mark Niklas Müller, Yuhao Mao, Maximilian Baader, Marc Fischer, and Martin
 536 Vechev. [Gaussian Loss Smoothing Enables Certified Training with Tight Convex Relaxations](#).
 537 *Transactions on Machine Learning Research*, 2025.

540 Mislav Balunovic and Martin Vechev. Adversarial training and provable defenses: Bridging the gap.
 541 In *International Conference on Learning Representations*, 2020.
 542

543 Battista Biggio, Igino Corona, Davide Maiorca, Blaine Nelson, Nedim Šrndić, Pavel Laskov, Giorgio
 544 Giacinto, and Fabio Roli. Evasion attacks against machine learning at test time. In *European Con-
 545 ference on Machine Learning and Principles and Practice of Knowledge Discovery in Databases
 546 (ECML PKDD)*, 2013.

547 Rudy Bunel, Ilker Turcaslan, Philip HS Torr, Pushmeet Kohli, and M Pawan Kumar. A unified view
 548 of piecewise linear neural network verification. In *Neural Information Processing Systems*, 2018.
 549

550 Rudy Bunel, Alessandro De Palma, Alban Desmaison, Krishnamurthy Dvijotham, Pushmeet Kohli,
 551 Philip HS Torr, and M Pawan Kumar. Lagrangian decomposition for neural network verification.
 552 In *Conference on Uncertainty in Artificial Intelligence*, 2020a.

553 Rudy Bunel, Jingyue Lu, Ilker Turcaslan, P Kohli, P Torr, and M Pawan Kumar. Branch and bound
 554 for piecewise linear neural network verification. *Journal of Machine Learning Research*, 21(2020),
 555 2020b.

556 Tianlong Chen, Zhenyu Zhang, Sijia Liu, Shiyu Chang, and Zhangyang Wang. Robust overfitting
 557 may be mitigated by properly learned smoothening. In *International Conference on Learning
 558 Representations*, 2020.

559 Patryk Chrabaszcz, Ilya Loshchilov, and Frank Hutter. A downsampled variant of ImageNet as an
 560 alternative to the CIFAR datasets. *arXiv:1707.08819*, 2017.

562 Jeremy Cohen, Elan Rosenfeld, and Zico Kolter. Certified adversarial robustness via randomized
 563 smoothing. In *International Conference on Machine Learning*, 2019.

564 Francesco Croce and Matthias Hein. [Reliable evaluation of adversarial robustness with an ensemble
 565 of diverse parameter-free attacks](#). In *International Conference on Machine Learning*, 2020.

567 Francesco Croce, Maksym Andriushchenko, and Matthias Hein. [Provable robustness of relu networks
 568 via maximization of linear regions](#). In *Conference on Artificial Intelligence and Statistics*. PMLR,
 569 2019.

570 Francesco Croce, Maksym Andriushchenko, Vikash Sehwag, Edoardo Debenedetti, Nicolas Flam-
 571 marion, Mung Chiang, Prateek Mittal, and Matthias Hein. Robustbench: a standardized adversarial
 572 robustness benchmark. In *Neural Information Processing Systems, Datasets and Benchmarks
 573 Track*, 2021.

575 Pau de Jorge, Adel Bibi, Riccardo Volpi, Amartya Sanyal, Philip Torr, Grégory Rogez, and Puneet K.
 576 Dokania. Make some noise: Reliable and efficient single-step adversarial training. In *Advances in
 577 Neural Information Processing Systems*, 2022.

578 Alessandro De Palma, Rudy Bunel, Alban Desmaison, Krishnamurthy Dvijotham, Pushmeet Kohli,
 579 Philip HS Torr, and M Pawan Kumar. Improved branch and bound for neural network verification
 580 via Lagrangian decomposition. *arXiv preprint arXiv:2104.06718*, 2021.

582 Alessandro De Palma, Rudy Bunel, Krishnamurthy Dvijotham, M. Pawan Kumar, and Robert
 583 Stanforth. IBP regularization for verified adversarial robustness via branch-and-bound. In *ICML
 584 2022 Workshop on Formal Verification of Machine Learning*, 2022.

585 Alessandro De Palma, Harkirat Singh Behl, Rudy Bunel, Philip H. S. Torr, and M. Pawan Kumar.
 586 Scaling the convex barrier with sparse dual algorithms. *Journal of Machine Learning Research*,
 587 2024a.

588 Alessandro De Palma, Rudy Bunel, Krishnamurthy Dvijotham, M. Pawan Kumar, Robert Stanforth,
 589 and Alessio Lomuscio. Expressive losses for verified robustness via convex combinations. In
 590 *International Conference on Learning Representations*, 2024b.

592 Krishnamurthy Dvijotham, Robert Stanforth, Sven Gowal, Timothy Mann, and Pushmeet Kohli. A
 593 dual approach to scalable verification of deep networks. In *Conference on Uncertainty in Artificial
 Intelligence*, 2018.

594 Ruediger Ehlers. Formal verification of piece-wise linear feed-forward neural networks. *Automated*
 595 *Technology for Verification and Analysis*, 2017.
 596

597 Claudio Ferrari, Mark Niklas Mueller, Nikola Jovanović, and Martin Vechev. Complete verification
 598 via multi-neuron relaxation guided branch-and-bound. In *International Conference on Learning*
 599 *Representations*, 2022.

600 Tommaso Furlanello, Zachary Lipton, Michael Tschannen, Laurent Itti, and Anima Anandkumar.
 601 Born again neural networks. In *International Conference on Machine Learning*, 2018.
 602

603 Sara Ghazanfari, Alexandre Araujo, Prashanth Krishnamurthy, Farshad Khorrami, and Siddharth
 604 Garg. Lipsim: A provably robust perceptual similarity metric. In *International Conference on*
 605 *Learning Representations*, 2024.

606 Micah Goldblum, Liam Fowl, Soheil Feizi, and Tom Goldstein. Adversarially robust distillation. In
 607 *AAAI conference on artificial intelligence*, 2020.
 608

609 Ian J. Goodfellow, Jonathon Shlens, and Christian Szegedy. Explaining and harnessing adversarial
 610 examples. In *International Conference on Learning Representations*, 2015.
 611

612 Sven Gowal, Krishnamurthy Dj Dvijotham, Robert Stanforth, Rudy Bunel, Chongli Qin, Jonathan
 613 Uesato, Relja Arandjelovic, Timothy Mann, and Pushmeet Kohli. Scalable verified training for
 614 provably robust image classification. In *Proceedings of the IEEE/CVF International Conference*
 615 *on Computer Vision*, 2019.

616 Kaiming He, Xiangyu Zhang, Shaoqing Ren, and Jian Sun. Identity mappings in deep residual
 617 networks. In *European Conference on Computer Vision (ECCV)*, 2016.
 618

619 P. Henriksen and A. Lomuscio. Deepsplit: An efficient splitting method for neural network verification
 620 via indirect effect analysis. In *Proceedings of the 30th International Joint Conference on Artificial*
 621 *Intelligence (IJCAI21)*, 2021.

622 Byeongho Heo, Jeesoo Kim, Sangdoo Yun, Hyojin Park, Nojun Kwak, and Jin Young Choi. A
 623 comprehensive overhaul of feature distillation. In *International Conference on Computer Vision*,
 624 2019.
 625

626 Timothy Hickey, Qun Ju, and Maarten H Van Emden. Interval arithmetic: From principles to
 627 implementation. *Journal of the ACM (JACM)*, 2001.
 628

629 Geoffrey Hinton, Oriol Vinyals, and Jeff Dean. Distilling the knowledge in a neural network. *arXiv*
 630 *preprint arXiv:1503.02531*, 2015.
 631

632 Kai Hu, Andy Zou, Zifan Wang, Klas Leino, and Matt Fredrikson. Unlocking deterministic robustness
 633 certification on imangenet. In *Neural Information Processing Systems*, 2023.
 634

635 Patrick Indri, Peter Blohm, Anagha Athavale, Ezio Bartocci, Georg Weissenbacher, Matteo Maffei,
 636 Dejan Nickovic, Thomas Gärtner, and Sagar Malhotra. Distillation based robustness verification
 637 with pac guarantees. In *ICML 2024 Next Generation of AI Safety Workshop*, 2024.

638 Nikola Jovanović, Mislav Balunović, Maximilian Baader, and Martin T. Vechev. On the paradox of
 639 certified training. *Transactions on Machine Learning Research*, 2022.
 640

641 Guy Katz, Clark Barrett, David Dill, Kyle Julian, and Mykel Kochenderfer. Reluplex: An efficient
 642 SMT solver for verifying deep neural networks. In *Computer Aided Verification*, 2017.
 643

644 Diederik P. Kingma and Jimmy Ba. Adam: A method for stochastic optimization. In *International*
 645 *Conference on Learning Representations*, 2015.
 646

647 A. Krizhevsky and G. Hinton. Learning multiple layers of features from tiny images. *Master's thesis*,
 648 *Department of Computer Science, University of Toronto*, 2009.
 649

650 Ya Le and Xuan S. Yang. Tiny imangenet visual recognition challenge. 2015.

648 Sungyoon Lee, Woojin Lee, Jinseong Park, and Jaewook Lee. Towards better understanding of
 649 training certifiably robust models against adversarial examples. In *Neural Information Processing*
 650 *Systems*, 2021.

651 Klas Leino, Zifan Wang, and Matt Fredrikson. Globally-robust neural networks. In *International*
 652 *Conference on Machine Learning*, PMLR.

653 Chen Liu, Mathieu Salzmann, and Sabine Süsstrunk. [Training provably robust models by polyhedral](#)
 654 [envelope regularization](#). *IEEE Transactions on Neural Networks and Learning Systems*, 34(6),
 655 2021.

656 Alessio Lomuscio and Lalit Maganti. An approach to reachability analysis for feed-forward ReLU
 657 neural networks. *arXiv:1706.07351*, 2017.

658 Aleksander Madry, Aleksandar Makelov, Ludwig Schmidt, Dimitris Tsipras, and Adrian Vladu.
 659 Towards deep learning models resistant to adversarial attacks. In *International Conference on*
 660 *Learning Representations*, 2018.

661 Yuhao Mao, Mark Niklas Müller, Marc Fischer, and Martin Vechev. TAPS: Connecting certified and
 662 adversarial training. In *Neural Information Processing Systems*, 2023.

663 Yuhao Mao, Mark Niklas Müller, Marc Fischer, and Martin Vechev. Understanding certified training
 664 with interval bound propagation. In *International Conference on Learning Representations*, 2024a.

665 Yuhao Mao, Yani Zhang, and Martin Vechev. [On the Expressiveness of Multi-Neuron Convex](#)
 666 [Relaxations](#). *arXiv preprint arXiv:2410.06816*, 2024b.

667 Yuhao Mao, Stefan Balaucă, and Martin Vechev. CTBench: A library and benchmark for certified
 668 training. In *International Conference on Machine Learning*, 2025.

669 Laurent Meunier, Blaise J Delattre, Alexandre Araujo, and Alexandre Allauzen. A dynamical system
 670 perspective for Lipschitz neural networks. In *International Conference on Machine Learning*,
 671 2022.

672 Matthew Mirman, Timon Gehr, and Martin Vechev. Differentiable abstract interpretation for provably
 673 robust neural networks. In *International Conference on Machine Learning*, 2018.

674 Awais Muhammad, Fengwei Zhou, Chuanlong Xie, Jiawei Li, Sung-Ho Bae, and Zhenguo Li.
 675 Mixacm: Mixup-based robustness transfer via distillation of activated channel maps. 2021.

676 Mark Niklas Müller, Franziska Eckert, Marc Fischer, and Martin Vechev. Certified training: Small
 677 boxes are all you need. In *International Conference on Learning Representations*, 2023.

678 Adam Paszke, Sam Gross, Francisco Massa, Adam Lerer, James Bradbury, Gregory Chanan, Trevor
 679 Killeen, Zeming Lin, Natalia Gimelshein, Luca Antiga, Alban Desmaison, Andreas Kopf, Edward
 680 Yang, Zachary DeVito, Martin Raison, Alykhan Tejani, Sasank Chilamkurthy, Benoit Steiner,
 681 Lu Fang, Junjie Bai, and Soumith Chintala. Pytorch: An imperative style, high-performance deep
 682 learning library. In *Neural Information Processing Systems*, 2019.

683 Bernd Prach, Fabio Brau, Giorgio Buttazzo, and Christoph H Lampert. 1-lipschitz layers compared:
 684 Memory speed and certifiable robustness. In *IEEE/CVF Conference on Computer Vision and*
 685 *Pattern Recognition*, 2024.

686 Adriana Romero, Nicolas Ballas, Samira Ebrahimi Kahou, Antoine Chassang, Carlo Gatta, and
 687 Yoshua Bengio. Fitnets: Hints for thin deep nets. In *International Conference on Learning*
 688 *Representations*, 2015.

689 Zhouxing Shi, Yihan Wang, Huan Zhang, Jinfeng Yi, and Cho-Jui Hsieh. Fast certified robust training
 690 with short warmup. In *Neural Information Processing Systems*, 2021.

691 Gagandeep Singh, Timon Gehr, Markus Püschel, and Martin Vechev. An abstract domain for
 692 certifying neural networks. In *Proceedings of the ACM on Programming Languages*, 2019.

693 Teruo Sunaga. Theory of an interval algebra and its application to numerical analysis. *RAAG Memoirs*,
 694 1958.

702 Christian Szegedy, Wojciech Zaremba, Ilya Sutskever, Joan Bruna, Dumitru Erhan, Ian J. Goodfellow,
 703 and Rob Fergus. Intriguing properties of neural networks. In *International Conference on Learning
 704 Representations*, 2014.

705 Vincent Tjeng, Kai Xiao, and Russ Tedrake. Evaluating robustness of neural networks with mixed
 706 integer programming. *International Conference on Learning Representations*, 2019.

708 Pratik Vaishnavi, Veena Krish, Farhan Ahmed, Kevin Eykholt, and Amir Rahmati. On the feasibility
 709 of compressing certifiably robust neural networks. In *Workshop on Trustworthy and Socially
 710 Responsible Machine Learning, NeurIPS 2022*, 2022.

711 Shiqi Wang, Huan Zhang, Kaidi Xu, Xue Lin, Suman Jana, Cho-Jui Hsieh, and J Zico Kolter.
 712 Beta-CROWN: Efficient bound propagation with per-neuron split constraints for complete and
 713 incomplete neural network verification. In *Neural Information Processing Systems*, 2021.

714 Eric Wong and Zico Kolter. Provable defenses against adversarial examples via the convex outer
 715 adversarial polytope. In *International Conference on Machine Learning*, 2018.

717 Kai Xiao, Vincent Tjeng, Nur Muhammad Shafiullah, and Aleksander Madry. Training for faster
 718 adversarial robustness verification via inducing relu stability. *International Conference on Learning
 719 Representations*, 2019.

720 Kaidi Xu, Zhouxing Shi, Huan Zhang, Yihan Wang, Kai-Wei Chang, Minlie Huang, Bhavya
 721 Kailkhura, Xue Lin, and Cho-Jui Hsieh. Automatic perturbation analysis for scalable certified
 722 robustness and beyond. In *Neural Information Processing Systems*, 2020.

724 Kaidi Xu, Huan Zhang, Shiqi Wang, Yihan Wang, Suman Jana, Xue Lin, and Cho-Jui Hsieh. Fast
 725 and complete: Enabling complete neural network verification with rapid and massively parallel
 726 incomplete verifiers. In *International Conference on Learning Representations*, 2021.

727 Sergey Zagoruyko and Nikos Komodakis. Paying more attention to attention: Improving the
 728 performance of convolutional neural networks via attention transfer. In *International Conference
 729 on Learning Representations*, 2017.

730 Bohang Zhang, Tianle Cai, Zhou Lu, Di He, and Liwei Wang. Towards certifying l-infinity robustness
 731 using neural networks with l-inf-dist neurons. In *International Conference on Machine Learning*,
 732 2021.

733 Bohang Zhang, Du Jiang, Di He, and Liwei Wang. Boosting the certified robustness of l-infinity
 734 distance nets. In *International Conference on Learning Representations*, 2022a.

736 Bohang Zhang, Du Jiang, Di He, and Liwei Wang. Rethinking lipschitz neural networks and certified
 737 robustness: A boolean function perspective. In *Neural Information Processing Systems*, 2022b.

738 Huan Zhang, Tsui-Wei Weng, Pin-Yu Chen, Cho-Jui Hsieh, and Luca Daniel. Efficient neural network
 739 robustness certification with general activation functions. In *Neural Information Processing
 740 Systems*, 2018.

742 Huan Zhang, Hongge Chen, Chaowei Xiao, Sven Gowal, Robert Stanforth, Bo Li, Duane Boning,
 743 and Cho-Jui Hsieh. Towards stable and efficient training of verifiably robust neural networks. In
 744 *International Conference on Learning Representations*, 2020.

745 Huan Zhang, Shiqi Wang, Kaidi Xu, Linyi Li, Bo Li, Suman Jana, Cho-Jui Hsieh, and J Zico
 746 Kolter. General cutting planes for bound-propagation-based neural network verification. In *Neural
 747 Information Processing Systems*, 2022c.

748 Duo Zhou, Christopher Brix, Grani A Hanusanto, and Huan Zhang. Scalable neural network
 749 verification with branch-and-bound inferred cutting planes. In *Neural Information Processing
 750 Systems*, 2024.

752 Jianing Zhu, Jiangchao Yao, Bo Han, Jingfeng Zhang, Tongliang Liu, Gang Niu, Jingren Zhou,
 753 Jianliang Xu, and Hongxia Yang. Reliable adversarial distillation with unreliable teachers. In
 754 *International Conference on Learning Representations*, 2022.

755 Bojia Zi, Shihao Zhao, Xingjun Ma, and Yu-Gang Jiang. Revisiting adversarial robustness distillation:
 Robust soft labels make student better. In *International Conference on Computer Vision*, 2021.

756 **A INTERVAL BOUND PROPAGATION**
757

758 We here provide details concerning the computations of IBP bounds omitted from §2.1. Assuming a
759 feed-forward network structure, let W^j and b^j respectively be the weight and bias of the j -th layer, and
760 let σ denote a monotonic element-wise activation function, which, as stated in §2, we assume to be the
761 ReLU activation in this work. Furthermore, let $\tilde{W}^n := ({}_y I^k - I^k) W^n$ and $\tilde{b}^n := ({}_y I^k - I^k) b^n$
762 denote the weight and bias corresponding to the composition of the last network layer and of
763 the difference between logits. IBP proceeds by first computing $\hat{1}^1 = W^1 \mathbf{x} - \epsilon |W^1| \mathbf{1} + \mathbf{b}^1$ and
764 $\hat{\mathbf{u}}^1 = W^1 \mathbf{x} + \epsilon |W^1| \mathbf{1} + \mathbf{b}^1$, and then derives $\underline{z}_{f_\theta}^{\mathcal{C}_\epsilon}(\mathbf{x}, y)$ by iteratively computing lower and upper
765 bounds ($\hat{1}^j$, and $\hat{\mathbf{u}}^j$, respectively) to the network pre-activations at layer j :

$$\begin{aligned} 767 \underline{z}_{f_\theta}^{\mathcal{C}_\epsilon}(\mathbf{x}, y) &= [\tilde{W}^n]_+ \sigma(\hat{1}^{n-1}) + [\tilde{W}^n]_- \sigma(\hat{\mathbf{u}}^{n-1}) + \tilde{b}^n, \quad \text{where:} \\ 768 \hat{1}^j &= [W^j]_+ \sigma(\hat{1}^{j-1}) + \frac{1}{2} [W^j]_- \sigma(\hat{\mathbf{u}}^{j-1}) + \mathbf{b}_j \\ 769 \hat{\mathbf{u}}^j &= [W^j]_+ \sigma(\hat{\mathbf{u}}^{j-1}) + \frac{1}{2} [W^j]_- \sigma(\hat{1}^{j-1}) + \mathbf{b}_j \end{aligned} \quad (11)$$

772 **B PROOFS OF TECHNICAL RESULTS**
773

774 We here provide the proofs omitted from §3.

775 *Remark B.1.* Let $f : \mathbb{R}^n \rightarrow \mathbb{R}$. If $\mathcal{A} \neq \emptyset$ and $\mathcal{A} \subseteq \mathcal{B}$, then $\max_{\mathbf{x} \in \mathcal{A}} f(\mathbf{x}) \leq \max_{\mathbf{x} \in \mathcal{B}} f(\mathbf{x})$.

776 **Proposition 3.1.** Let $\underline{h}_{\theta_h}^{\mathcal{C}_\epsilon}(\mathbf{x})$ and $\bar{h}_{\theta_h}^{\mathcal{C}_\epsilon}(\mathbf{x})$ respectively denote IBP lower and upper bounds to the
777 student features:

$$778 \underline{h}_{\theta_h}^{\mathcal{C}_\epsilon}(\mathbf{x}) \leq h_{\theta_h}(\mathbf{x}') \leq \bar{h}_{\theta_h}^{\mathcal{C}_\epsilon}(\mathbf{x}), \quad \forall \mathbf{x}' \in \mathcal{C}_\epsilon(\mathbf{x}).$$

779 The loss function $\bar{\mathcal{R}}_{f_\theta}^{\mathcal{C}_\epsilon}(\mathbf{x}, y) := \sum_i \max \left\{ \left(\underline{h}_{\theta_h}^{\mathcal{C}_\epsilon}(\mathbf{x})_i - h_{\theta_h}^t(\mathbf{x})_i \right)^2, \left(\bar{h}_{\theta_h}^{\mathcal{C}_\epsilon}(\mathbf{x})_i - h_{\theta_h}^t(\mathbf{x})_i \right)^2 \right\}$ is an
780 upper bound to the worst-case distillation loss from equation (8): $\bar{\mathcal{R}}_{f_\theta}^{\mathcal{C}_\epsilon}(\mathbf{x}, y) \geq \mathcal{R}_{f_\theta}^{\mathcal{C}_\epsilon}(\mathbf{x}, y)$.

781 *Proof.* Let us start by upper bounding the worst-case distillation loss $\mathcal{R}_{f_\theta}^{\mathcal{C}_\epsilon}(\mathbf{x}, y)$:

$$\begin{aligned} 782 \mathcal{R}_{f_\theta}^{\mathcal{C}_\epsilon}(\mathbf{x}, y) &= \max_{\mathbf{x}' \in \mathcal{C}_\epsilon(\mathbf{x})} \left\| h_{\theta_h}(\mathbf{x}') - h_{\theta_h}^t(\mathbf{x}) \right\|_2^2 = \max_{\mathbf{x}' \in \mathcal{C}_\epsilon(\mathbf{x})} \left[\sum_i \left(h_{\theta_h}(\mathbf{x}')_i - h_{\theta_h}^t(\mathbf{x})_i \right)^2 \right] \\ 783 &\leq \sum_i \max_{\mathbf{x}' \in \mathcal{C}_\epsilon(\mathbf{x})} \left(h_{\theta_h}(\mathbf{x}')_i - h_{\theta_h}^t(\mathbf{x})_i \right)^2. \end{aligned}$$

784 Let $\mathcal{M}_i = \left\{ h_{\theta_h}(\mathbf{x}')_i \mid \mathbf{x}' \in \operatorname{argmax}_{\mathbf{x}' \in \mathcal{C}_\epsilon(\mathbf{x})} \left(h_{\theta_h}(\mathbf{x}')_i - h_{\theta_h}^t(\mathbf{x})_i \right)^2 \right\}$. By the definition of the
785 IBP feature bounds $\underline{h}_{\theta_h}^{\mathcal{C}_\epsilon}(\mathbf{x})$ and $\bar{h}_{\theta_h}^{\mathcal{C}_\epsilon}(\mathbf{x})$:

$$786 \mathcal{M}_i \subseteq \left[\underline{h}_{\theta_h}^{\mathcal{C}_\epsilon}(\mathbf{x})_i, \bar{h}_{\theta_h}^{\mathcal{C}_\epsilon}(\mathbf{x})_i \right].$$

787 Recalling remark B.1, we can hence further bound $\mathcal{R}_{f_\theta}^{\mathcal{C}_\epsilon}(\mathbf{x}, y)$ as follows:

$$\begin{aligned} 788 \mathcal{R}_{f_\theta}^{\mathcal{C}_\epsilon}(\mathbf{x}, y) &\leq \sum_i \max_{\mathbf{x}' \in \mathcal{C}_\epsilon(\mathbf{x})} \left(h_{\theta_h}(\mathbf{x}')_i - h_{\theta_h}^t(\mathbf{x})_i \right)^2 = \sum_i \max_{h \in \mathcal{M}_i} \left(h - h_{\theta_h}^t(\mathbf{x})_i \right)^2 \\ 789 &\leq \sum_i \max_{h \in \left[\underline{h}_{\theta_h}^{\mathcal{C}_\epsilon}(\mathbf{x})_i, \bar{h}_{\theta_h}^{\mathcal{C}_\epsilon}(\mathbf{x})_i \right]} \left(h - h_{\theta_h}^t(\mathbf{x})_i \right)^2. \end{aligned}$$

800 Let us note that (for any $b, l, u \in \mathbb{R}$, $l \leq u$):

$$801 \max_{x \in [l, u]} (x - b)^2 = \max \left\{ (l - b)^2, (u - b)^2 \right\}. \quad (12)$$

802 We can hence write $\mathcal{R}_{f_\theta}^{\mathcal{C}_\epsilon}(\mathbf{x}, y) \leq \bar{\mathcal{R}}_{f_\theta}^{\mathcal{C}_\epsilon}(\mathbf{x}, y)$. □

810 **Proposition 3.2.** *The loss function*

811

$$812 \quad {}^{CC}\mathcal{R}_{f_\theta}^{\mathcal{C}_\epsilon}(\alpha; \mathbf{x}, y) := \sum_i \max \left\{ \left({}^{CC}\underline{h}_{\theta_h}^{\mathcal{C}_\epsilon}(\alpha; \mathbf{x})_i - h_{\theta_h^t}^t(\mathbf{x})_i \right)^2, \left({}^{CC}\bar{h}_{\theta_h}^{\mathcal{C}_\epsilon}(\alpha; \mathbf{x})_i - h_{\theta_h^t}^t(\mathbf{x})_i \right)^2 \right\}$$

813

814 *enjoys the following properties:*

815

816 1. ${}^{CC}\mathcal{R}_{f_\theta}^{\mathcal{C}_\epsilon}(0; \mathbf{x}, y) = \mathcal{R}_{f_\theta}^{\mathcal{C}_\epsilon}(\mathbf{x}, y)$ and ${}^{CC}\mathcal{R}_{f_\theta}^{\mathcal{C}_\epsilon}(1; \mathbf{x}, y) = \bar{\mathcal{R}}_{f_\theta}^{\mathcal{C}_\epsilon}(\mathbf{x}, y);$

817 2. $\mathcal{R}_{f_\theta}^{\mathcal{C}_\epsilon}(\mathbf{x}, y) \leq {}^{CC}\mathcal{R}_{f_\theta}^{\mathcal{C}_\epsilon}(\alpha; \mathbf{x}, y) \leq \bar{\mathcal{R}}_{f_\theta}^{\mathcal{C}_\epsilon}(\mathbf{x}, y) \forall \alpha \in [0, 1];$

818 3. ${}^{CC}\mathcal{R}_{f_\theta}^{\mathcal{C}_\epsilon}(\alpha; \mathbf{x}, y)$ is continuous and monotonically increasing for $\alpha \in [0, 1].$

819

820 *Proof.* Let us define $\mathcal{I}_i^\alpha := \left[{}^{CC}\underline{h}_{\theta_h}^{\mathcal{C}_\epsilon}(\alpha; \mathbf{x})_i, {}^{CC}\bar{h}_{\theta_h}^{\mathcal{C}_\epsilon}(\alpha; \mathbf{x})_i \right].$ Owing to equation (12), we can write
821 the following alternative definition of ${}^{CC}\mathcal{R}_{f_\theta}^{\mathcal{C}_\epsilon}(\alpha; \mathbf{x}, y):$

822

$$823 \quad {}^{CC}\mathcal{R}_{f_\theta}^{\mathcal{C}_\epsilon}(\alpha; \mathbf{x}, y) = \sum_i \max_{h \in \mathcal{I}_i^\alpha} \left(h - h_{\theta_h^t}^t(\mathbf{x})_i \right)^2. \quad (13)$$

824

825 Let us recall that ${}^{CC}\bar{h}_{\theta_h}^{\mathcal{C}_\epsilon}(\alpha; \mathbf{x}) := (1 - \alpha) h_{\theta_h}(\mathbf{x}_{\text{adv}}) + \alpha \bar{h}_{\theta_h}^{\mathcal{C}_\epsilon}(\mathbf{x}),$ and
826 ${}^{CC}\underline{h}_{\theta_h}^{\mathcal{C}_\epsilon}(\alpha; \mathbf{x}) := (1 - \alpha) h_{\theta_h}(\mathbf{x}_{\text{adv}}) + \alpha \underline{h}_{\theta_h}^{\mathcal{C}_\epsilon}(\mathbf{x}).$ By pointing out that $h_{\theta_h}(\mathbf{x}_{\text{adv}}) \in \left[\underline{h}_{\theta_h}^{\mathcal{C}_\epsilon}(\mathbf{x}), \bar{h}_{\theta_h}^{\mathcal{C}_\epsilon}(\mathbf{x}) \right],$
827 we can see that, $\forall \alpha \in [0, 1]:$

828

$$829 \quad \underline{h}_{\theta_h}^{\mathcal{C}_\epsilon}(\mathbf{x}) \leq {}^{CC}\underline{h}_{\theta_h}^{\mathcal{C}_\epsilon}(\alpha; \mathbf{x}) \leq h_{\theta_h}(\mathbf{x}_{\text{adv}}), \quad h_{\theta_h}(\mathbf{x}_{\text{adv}}) \leq {}^{CC}\bar{h}_{\theta_h}^{\mathcal{C}_\epsilon}(\alpha; \mathbf{x}) \leq \bar{h}_{\theta_h}^{\mathcal{C}_\epsilon}(\mathbf{x}).$$

830

831 Consequently, $\forall \alpha \in [0, 1]$ and $\forall i \in \llbracket 1, m \rrbracket$ (m being the dimensionality of the feature space):

832

$$833 \quad \mathcal{I}_i^0 = \{h_{\theta_h}(\mathbf{x}_{\text{adv}})_i\} \subseteq \mathcal{I}_i^\alpha \subseteq \left[\underline{h}_{\theta_h}^{\mathcal{C}_\epsilon}(\mathbf{x})_i, \bar{h}_{\theta_h}^{\mathcal{C}_\epsilon}(\mathbf{x})_i \right] = \mathcal{I}_i^1.$$

834

835 And hence, as per remark B.1:

836

$$837 \quad \sum_i \max_{h \in \mathcal{I}_i^0} \left(h - h_{\theta_h^t}^t(\mathbf{x})_i \right)^2 \leq \sum_i \max_{h \in \mathcal{I}_i^\alpha} \left(h - h_{\theta_h^t}^t(\mathbf{x})_i \right)^2 \leq \sum_i \max_{h \in \mathcal{I}_i^1} \left(h - h_{\theta_h^t}^t(\mathbf{x})_i \right)^2. \quad (14)$$

838

839 Using equation (13) with $\alpha = 0$ we can see that:

840

$$841 \quad {}^{CC}\mathcal{R}_{f_\theta}^{\mathcal{C}_\epsilon}(0; \mathbf{x}, y) = \sum_i \max_{h \in \mathcal{I}_i^0} \left(h - h_{\theta_h^t}^t(\mathbf{x})_i \right)^2 = \sum_i \left(h_{\theta_h}(\mathbf{x}_{\text{adv}})_i - h_{\theta_h^t}^t(\mathbf{x})_i \right)^2$$

842

$$843 \quad = \left\| h_{\theta_h}(\mathbf{x}_{\text{adv}}) - h_{\theta_h^t}^t(\mathbf{x}) \right\|_2^2 = \mathcal{R}_{f_\theta}^{\mathcal{C}_\epsilon}(\mathbf{x}, y).$$

844

845 Using it again with $\alpha = 1$ and recalling equation (12), we obtain:

846

$$847 \quad {}^{CC}\mathcal{R}_{f_\theta}^{\mathcal{C}_\epsilon}(1; \mathbf{x}, y) = \sum_i \max_{h \in \mathcal{I}_i^1} \left(h - h_{\theta_h^t}^t(\mathbf{x})_i \right)^2 =$$

848

$$849 \quad = \sum_i \max \left\{ \left(\underline{h}_{\theta_h}^{\mathcal{C}_\epsilon}(\mathbf{x})_i - h_{\theta_h^t}^t(\mathbf{x})_i \right)^2, \left(\bar{h}_{\theta_h}^{\mathcal{C}_\epsilon}(\mathbf{x})_i - h_{\theta_h^t}^t(\mathbf{x})_i \right)^2 \right\} = \bar{\mathcal{R}}_{f_\theta}^{\mathcal{C}_\epsilon}(\mathbf{x}, y),$$

850

851 Hence proving the first point of the proposition.

852

853 The second point can be now proved by again using equation (13) within equation (14):

854

$$855 \quad \mathcal{R}_{f_\theta}^{\mathcal{C}_\epsilon}(\mathbf{x}, y) = {}^{CC}\mathcal{R}_{f_\theta}^{\mathcal{C}_\epsilon}(0; \mathbf{x}, y) \leq {}^{CC}\mathcal{R}_{f_\theta}^{\mathcal{C}_\epsilon}(\alpha; \mathbf{x}, y) \leq {}^{CC}\mathcal{R}_{f_\theta}^{\mathcal{C}_\epsilon}(1; \mathbf{x}, y) = \bar{\mathcal{R}}_{f_\theta}^{\mathcal{C}_\epsilon}(\mathbf{x}, y).$$

856

857 Concerning the third point, the continuity of ${}^{CC}\mathcal{R}_{f_\theta}^{\mathcal{C}_\epsilon}(\alpha; \mathbf{x}, y)$ for $\alpha \in [0, 1]$ can be proved by pointing
858 out that ${}^{CC}\mathcal{R}_{f_\theta}^{\mathcal{C}_\epsilon}(\alpha; \mathbf{x}, y)$ is composed of operators preserving continuity (pointwise max), linear
859 combinations and compositions of continuous functions of $\alpha.$ In order to prove monotonicity, note that,

860

864 for any $\alpha, \alpha' \in [0, 1]$ with $\alpha \leq \alpha'$, ${}^{CC}\bar{h}_{\theta_h}^{\mathcal{C}_\epsilon}(\alpha'; \mathbf{x}) \geq {}^{CC}\bar{h}_{\theta_h}^{\mathcal{C}_\epsilon}(\alpha; \mathbf{x})$ and ${}^{CC}h_{\theta_h}^{\mathcal{C}_\epsilon}(\alpha'; \mathbf{x}) \leq {}^{CC}h_{\theta_h}^{\mathcal{C}_\epsilon}(\alpha; \mathbf{x})$,
 865 implying $\mathcal{I}_i^\alpha \subseteq \mathcal{I}_i^{\alpha'}$. Hence, recalling remark B.1, for any $\alpha, \alpha' \in [0, 1]$ with $\alpha \leq \alpha'$, we have:
 866

$$868 {}^{CC}\mathcal{R}_{f_\theta}^{\mathcal{C}_\epsilon}(\alpha; \mathbf{x}, y) = \sum_i \max_{h \in \mathcal{I}_i^\alpha} (h - h_{\theta_h}^t(\mathbf{x})_i)^2 \leq \sum_i \max_{h \in \mathcal{I}_i^{\alpha'}} (h - h_{\theta_h}^t(\mathbf{x})_i)^2 = {}^{CC}\mathcal{R}_{f_\theta}^{\mathcal{C}_\epsilon}(\alpha'; \mathbf{x}, y),$$

871 which proves that ${}^{CC}\mathcal{R}_{f_\theta}^{\mathcal{C}_\epsilon}(\alpha; \mathbf{x}, y)$ is monotonically increasing for $\alpha \in [0, 1]$. \square
 872

874 **Lemma 3.3.** *Let the student classification head $g_{\theta_g}(\mathbf{a})$ be affine, and let $\tilde{g}_{\theta_g}^y(\mathbf{a}) := \tilde{W}^n \mathbf{a} + \tilde{\mathbf{b}}^n$ be
 875 its composition with the operator performing the difference between logits. We can write the CC-IBP
 876 convex combinations as:*

$$879 {}^{CC}\mathbf{z}_{f_\theta}^{\mathcal{C}_\epsilon}(\alpha; \mathbf{x}, y) = \begin{bmatrix} [\tilde{W}^n]_+ & [\tilde{W}^n]_- \end{bmatrix} \begin{bmatrix} {}^{CC}h_{\theta_h}^{\mathcal{C}_\epsilon}(\alpha; \mathbf{x}) \\ {}^{CC}\bar{h}_{\theta_h}^{\mathcal{C}_\epsilon}(\alpha; \mathbf{x}) \end{bmatrix} + \tilde{\mathbf{b}}^n.$$

884 *Proof.* We can write the student logit differences as: $\mathbf{z}_{f_\theta}(\mathbf{x}, y) = \tilde{W}^n h_{\theta_h}(\mathbf{x}) + \tilde{\mathbf{b}}^n$. Hence, given
 885 IBP bounds to the student features $h_{\theta_h}^{\mathcal{C}_\epsilon}(\mathbf{x})$ and $\bar{h}_{\theta_h}^{\mathcal{C}_\epsilon}(\mathbf{x})$ (corresponding to $\sigma(\hat{\mathbf{l}}^{n-1})$ and $\sigma(\hat{\mathbf{u}}^{n-1})$
 886 in equation (11), respectively), we can compute the logit differences lower bounds $\underline{\mathbf{z}}_{f_\theta}^{\mathcal{C}_\epsilon}(\mathbf{x}, y)$ as per
 887 equation (11):
 888

$$889 \underline{\mathbf{z}}_{f_\theta}^{\mathcal{C}_\epsilon}(\mathbf{x}, y) = [\tilde{W}^n]_+ h_{\theta_h}^{\mathcal{C}_\epsilon}(\mathbf{x}) + [\tilde{W}^n]_- \bar{h}_{\theta_h}^{\mathcal{C}_\epsilon}(\mathbf{x}) + \tilde{\mathbf{b}}^n.$$

892 Let us write the adversarial logit differences $\mathbf{z}_{f_\theta}(\mathbf{x}_{\text{adv}}, y)$ as a function of the adversarial
 893 student features:

$$895 \mathbf{z}_{f_\theta}(\mathbf{x}_{\text{adv}}, y) = \tilde{W}^n h_{\theta_h}(\mathbf{x}_{\text{adv}}) + \tilde{\mathbf{b}}^n = ([\tilde{W}^n]_+ + [\tilde{W}^n]_-) h_{\theta_h}(\mathbf{x}_{\text{adv}}) + \tilde{\mathbf{b}}^n.$$

897 Replacing the above two equations in the definition of the CC-IBP convex combinations
 898 ${}^{CC}\mathbf{z}_{f_\theta}^{\mathcal{C}_\epsilon}(\alpha; \mathbf{x}, y)$ (see §3.1) we get:
 899

$$900 {}^{CC}\mathbf{z}_{f_\theta}^{\mathcal{C}_\epsilon}(\alpha; \mathbf{x}, y) = (1 - \alpha) \mathbf{z}_{f_\theta}(\mathbf{x}_{\text{adv}}, y) + \alpha \underline{\mathbf{z}}_{f_\theta}^{\mathcal{C}_\epsilon}(\mathbf{x}, y) \\ 901 = (1 - \alpha) \left[([\tilde{W}^n]_+ + [\tilde{W}^n]_-) h_{\theta_h}(\mathbf{x}_{\text{adv}}) \right] + \alpha \left([\tilde{W}^n]_+ h_{\theta_h}^{\mathcal{C}_\epsilon}(\mathbf{x}) + [\tilde{W}^n]_- \bar{h}_{\theta_h}^{\mathcal{C}_\epsilon}(\mathbf{x}) \right) + \tilde{\mathbf{b}}^n \\ 902 = [\tilde{W}^n]_+ \left[(1 - \alpha) h_{\theta_h}(\mathbf{x}_{\text{adv}}) + \alpha h_{\theta_h}^{\mathcal{C}_\epsilon}(\mathbf{x}) \right] + [\tilde{W}^n]_- \left[(1 - \alpha) \bar{h}_{\theta_h}(\mathbf{x}_{\text{adv}}) + \alpha \bar{h}_{\theta_h}^{\mathcal{C}_\epsilon}(\mathbf{x}) \right] + \tilde{\mathbf{b}}^n.$$

906 Recalling that ${}^{CC}\bar{h}_{\theta_h}^{\mathcal{C}_\epsilon}(\alpha; \mathbf{x}) := (1 - \alpha) h_{\theta_h}(\mathbf{x}_{\text{adv}}) + \alpha \bar{h}_{\theta_h}^{\mathcal{C}_\epsilon}(\mathbf{x})$, and
 907 ${}^{CC}h_{\theta_h}^{\mathcal{C}_\epsilon}(\alpha; \mathbf{x}) := (1 - \alpha) h_{\theta_h}(\mathbf{x}_{\text{adv}}) + \alpha h_{\theta_h}^{\mathcal{C}_\epsilon}(\mathbf{x})$, we get:
 908

$$910 {}^{CC}\mathbf{z}_{f_\theta}^{\mathcal{C}_\epsilon}(\alpha; \mathbf{x}, y) = [\tilde{W}^n]_+ {}^{CC}h_{\theta_h}^{\mathcal{C}_\epsilon}(\alpha; \mathbf{x}) + [\tilde{W}^n]_- {}^{CC}\bar{h}_{\theta_h}^{\mathcal{C}_\epsilon}(\alpha; \mathbf{x}) + \tilde{\mathbf{b}}^n,$$

912 which concludes the proof. \square
 913

914 C PSEUDO-CODE

915 We here provide pseudo-code for CC-Dist: see algorithm 1.
 916

918

919

920

Algorithm 1 CC-Dist training loss $\mathcal{L}^{\text{CC-Dist}}(\alpha, 5/w; \mathbf{x}, y)$

921

922

923

924

925

926

927

928

929

930

931

932

933

934

935

1: **Input:** Student $f_{\theta} = g_{\theta_g} \circ h_{\theta_h}$, teacher feature map $h_{\theta_h}^t$, loss function \mathcal{L} , data point (\mathbf{x}, y) , perturbation set $\mathcal{C}_\epsilon(\mathbf{x})$, hyper-parameter α

2: Compute \mathbf{x}_{adv} via an adversarial attack on $\mathcal{C}_\epsilon(\mathbf{x})$

3: Compute $h_{\theta_h}^{\mathcal{C}_\epsilon}(\mathbf{x})$, $\bar{h}_{\theta_h}^{\mathcal{C}_\epsilon}(\mathbf{x})$ and $\mathbf{z}_{f_{\theta}}^{\mathcal{C}_\epsilon}(\mathbf{x}, y)$ via IBP

4: ${}^{\text{CC}}\bar{h}_{\theta_h}^{\mathcal{C}_\epsilon}(\alpha; \mathbf{x}) \leftarrow (1 - \alpha) h_{\theta_h}(\mathbf{x}_{\text{adv}}) + \alpha \bar{h}_{\theta_h}^{\mathcal{C}_\epsilon}(\mathbf{x})$

5: ${}^{\text{CC}}h_{\theta_h}^{\mathcal{C}_\epsilon}(\alpha; \mathbf{x}) \leftarrow (1 - \alpha) h_{\theta_h}(\mathbf{x}_{\text{adv}}) + \alpha h_{\theta_h}^{\mathcal{C}_\epsilon}(\mathbf{x})$

6: $\mathbf{z}_{f_{\theta}}(\mathbf{x}_{\text{adv}}, y) \leftarrow \left(g_{\theta_g}(h_{\theta_h}(\mathbf{x}_{\text{adv}}))_y \mathbf{1}^k - g_{\theta_g}(h_{\theta_h}(\mathbf{x}_{\text{adv}})) \right)$

7: ${}^{\text{CC}}\mathcal{L}_{f_{\theta}}^{\mathcal{C}_\epsilon}(\alpha; \mathbf{x}, y) \leftarrow \mathcal{L} \left(- \left[(1 - \alpha) \mathbf{z}_{f_{\theta}}(\mathbf{x}_{\text{adv}}, y) + \alpha \mathbf{z}_{f_{\theta}}^{\mathcal{C}_\epsilon}(\mathbf{x}, y) \right], y \right)$

8: ${}^{\text{CC}}\mathcal{R}_{f_{\theta}}^{\mathcal{C}_\epsilon}(\alpha; \mathbf{x}, y) \leftarrow \sum_i \max \left\{ \left({}^{\text{CC}}h_{\theta_h}^{\mathcal{C}_\epsilon}(\alpha; \mathbf{x})_i - h_{\theta_h}^t(\mathbf{x})_i \right)^2, \left({}^{\text{CC}}\bar{h}_{\theta_h}^{\mathcal{C}_\epsilon}(\alpha; \mathbf{x})_i - h_{\theta_h}^t(\mathbf{x})_i \right)^2 \right\}$

9: **return** ${}^{\text{CC}}\mathcal{L}_{f_{\theta}}^{\mathcal{C}_\epsilon}(\alpha; \mathbf{x}, y) + 5/w {}^{\text{CC}}\mathcal{R}_{f_{\theta}}^{\mathcal{C}_\epsilon}(\alpha; \mathbf{x}, y)$

936

D EXPERIMENTAL DETAILS

937

938

This appendix provides experimental details omitted from §5.

939

940

D.1 EXPERIMENTAL SETUP

941

Experiments were each carried out on an internal cluster using a single GPU and employing from 6 to 12 CPU cores. GPUs belonging to the following models were employed: Nvidia GTX 1080 Ti, Nvidia RTX 2080 Ti, Nvidia RTX 6000, Nvidia RTX 8000, Nvidia V100. CPU memory was capped at 10 GB for the training experiments, and at 100 GB for the verification experiments. The runtime of training runs ranges from roughly 5 hours for CIFAR-10, to roughly 4 days for downscaled ImageNet. For verification experiments, runtime ranges from below 8 hours for CIFAR-10 with $\epsilon = 8/255$ to roughly 12 days for downscaled ImageNet.

942

D.2 TRAINING SETUP AND HYPER-PARAMETERS

943

944

We now report the details of the employed training setup and hyper-parameters.

945

946

D.2.1 DATASETS

947

948

As stated in §5.1, the experiments were carried out on the following datasets: CIFAR-10 (Krizhevsky & Hinton, 2009), TinyImageNet (Le & Yang, 2015), and downscaled ImageNet (64×64) (Chrabaszcz et al., 2017). For all three, we train using random horizontal flips, random crops, and normalization as done in (De Palma et al., 2024b). The employed dataset splits comply with previous work in the area (De Palma et al., 2024b; Mao et al., 2023; Müller et al., 2023). Specifically, for CIFAR-10, which consists of 32×32 RGB images divided into 10 classes, we trained on the original 50,000 training points, and evaluated on the original 10,000 test points. For TinyImageNet, consisting of 64×64 RGB images and 200 classes, we trained on the original 100,000 training points, and evaluated on the original 10,000 validation images. Finally, for downscaled ImageNet, which consists of 64×64 RGB images and 1000 classes, we employed the original training set of 1,281,167 images, and evaluated on the original 50,000 validation images.

949

950

D.2.2 TRAINING SCHEDULES AND IMPLEMENTATION DETAILS

951

952

953

954

For CC-IBP, CC-Dist models and their teachers, trained networks are initialized using the specialized scheme by Shi et al. (2021), which reduces the magnitude of the IBP bounds. Teachers for CC-Dist are trained using pure adversarial training, relying on a 10-step PGD attack (Madry et al., 2018) with step size $\eta = 0.25\epsilon$. Complying with De Palma et al. (2024b), \mathbf{x}_{adv} for CC-Dist and CC-IBP models is computed using a single-step PGD attack with uniform random initialization and step size

972 $\eta = 10.0\epsilon$ on all setups except for CIFAR-10 with $\epsilon = 2/255$, which instead relies on a 8-step PGD
 973 attack with step size $\eta = 0.25\epsilon'$ run on a larger effective input perturbation ($\epsilon' = 2.1\epsilon$). All methods
 974 use a batch size of 128 throughout the experiments, and gradient clipping with norm equal to 10. We
 975 do not perform any early stopping.

976 As relatively common in the adversarial training literature (Andriushchenko & Flammarion, 2020;
 977 de Jorge et al., 2022), teachers for CC-Dist are trained using the SGD optimizer (with momentum
 978 set to 0.9), shorter schedules and a cyclic learning rate, which linearly increases the learning rate
 979 from 0 to 0.2 during the first half of the training, and then decreases it back to 0. As a longer number
 980 of teacher training epochs was found to be beneficial on TinyImageNet, we report it among the
 981 hyper-parameters in table 3. As instead common in the certified training literature, CC-Dist and
 982 CC-IBP models are trained using the Adam optimizer (Kingma & Ba, 2015) with longer training
 983 schedules and a learning rate of 5×10^{-4} , which is decayed twice by a factor 0.2. Their training
 984 starts with one epoch of “warm-up”, where the certified training loss is replaced by the standard
 985 cross entropy on the clean inputs, and proceeds with a “ramp-up” phase, during which the training
 986 perturbation radius ϵ is gradually increased from 0 to its target value, and the IBP regularization
 987 from Shi et al. (2021) is added to the training loss (with coefficient $\lambda = 0.5$ on CIFAR-10, and
 988 $\lambda = 0.2$ for TinyImageNet and downscaled ImageNet). Benchmark-specific details for CC-Dist
 989 models and CC-IBP, which are in accordance with De Palma et al. (2024b), follow:

- 990 • CIFAR-10 with $\epsilon = 2/255$: the CC-IBP and CC-Dist training schedule is 160-epochs long, with 80
 991 epochs of ramp-up, and with the learning rate decayed at epochs 120 and 140.
- 992 • CIFAR-10 with $\epsilon = 8/255$: 260 epochs, with 80 epochs of ramp-up, and with the learning rate
 993 decayed at epochs 180 and 220.
- 994 • TinyImageNet: 160 epochs, with 80 ramp-up epochs, and decaying the learning rate at epochs
 995 120 and 140.
- 996 • Downscaled ImageNet: 80 epochs, with 20 epochs of ramp-up, and decaying the learning rate at
 997 epochs 60 and 70.

999 In order to separate the effect of distillation from any other potential implementation detail, the CC-
 1000 IBP evaluations from table 1 were obtained by employing the CC-Dist implementation with $\beta = 0$.

1003 D.2.3 NETWORK ARCHITECTURE

1004 The employed CNN-7 architecture is left unvaried with respect to previous work (De Palma et al.,
 1005 2024b; Müller et al., 2023; Mao et al., 2023; 2025) except on downscaled ImageNet, where we
 1006 applied a small modification to the linear layers. Specifically, in order to make sure that the feature
 1007 space employed for distillation is larger than the network output space, we set the output size of the
 1008 penultimate layer (and the input size of the last) equal to 1024, instead of 512 as for the other datasets
 1009 and in De Palma et al. (2024b). As originally suggested by Shi et al. (2021) to improve performance,
 1010 and complying with previous work (De Palma et al., 2024b; Müller et al., 2023; Mao et al., 2023;
 1011 2025), we employ batch normalization (BatchNorm) after every network layer except the last. In
 1012 our implementation, adversarial attacks are carried out with the network in evaluation mode, hence
 1013 using the current BatchNorm running statistics. Except during the warm-up phase, where we also
 1014 perform an evaluation on the unperturbed data points, the network is exclusively evaluated on the
 1015 computed adversarial inputs \mathbf{x}_{adv} , which hence dominate the computed running statistics for most of
 1016 the training and for the final network. Finally, except for the clean loss during warm-up, which is
 1017 computed using the unperturbed current batch statistics, all the training loss computations (including
 1018 those requiring IBP bounds) are carried out using the batch statistics from the computed adversarial
 1019 inputs (hence in training mode).

1020 D.2.4 HYPER-PARAMETERS

1021 Table 3 reports a list of the main method and regularization hyper-parameter values for our evaluations
 1022 from table 1. As done in previous work (Gowal et al., 2019; Zhang et al., 2020; Shi et al., 2021;
 1023 Müller et al., 2023; De Palma et al., 2024b; Mao et al., 2025), and hence ensuring a fair comparison in
 1024 table 1, tuning was carried out directly on the evaluation sets. The details of the CC-Dist and CC-IBP
 1025 training schedules, taken from De Palma et al. (2024b), are instead reported in appendix D.2.2.

1026 Table 3: Hyper-parameter settings for the CC-Dist models from table 1, their respective teachers, and for our
 1027 CC-IBP evaluations reported in the same table.

1028	Dataset	ϵ	Method	α	ℓ_1	Teacher n. epochs	Teacher ℓ_1
1029 1030 1031 1032	CIFAR-10	$\frac{2}{255}$	CC-DIST	10^{-2}	3×10^{-6}	30	10^{-5}
			CC-IBP	10^{-2}	3×10^{-6}	/	/
	TinyImageNet	$\frac{8}{255}$	CC-DIST	0.5	0	30	5×10^{-6}
			CC-IBP	0.5	0	/	/
1033 1034 1035 1036 1037	TinyImageNet	$\frac{1}{255}$	CC-DIST	5×10^{-3}	5×10^{-5}	100	5×10^{-5}
			CC-IBP	3×10^{-3}	5×10^{-5}	/	/
	ImageNet64	$\frac{1}{255}$	CC-DIST	5×10^{-3}	10^{-5}	30	5×10^{-6}
			CC-IBP	5×10^{-3}	10^{-5}	/	/

1038
 1039
 1040 As explained in §3.3, we advocate for a constant distillation coefficient: we noticed that $\beta = 5/w$
 1041 yielded good performance across our earlier CIFAR-10 experiments, and then decided to keep it to the
 1042 same value across all evaluations. On CIFAR-10, we did not tune the α coefficient for either method:
 1043 it was set to be the CC-IBP α coefficient employed in De Palma et al. (2024b). Complying with
 1044 common practice in the certified training literature (De Palma et al., 2024b; Müller et al., 2023; Mao
 1045 et al., 2025), ℓ_1 regularization is applied on top of the employed training losses: the corresponding
 1046 values for CC-Dist and CC-IBP models were not tuned but taken from the CC-IBP values reported
 1047 in the expressive losses work (De Palma et al., 2024b). On TinyImageNet and ImageNet64, we
 1048 found that both the standard performance and the certified accuracy of CC-IBP could be significantly
 1049 improved compared to the original results from De Palma et al. (2024b), which respectively employ
 1050 $\alpha = 10^{-2}$ and $\alpha = 5 \times 10^{-2}$ for CC-IBP on TinyImageNet and ImageNet64, by decreasing α . In
 1051 particular, we selected the smallest α value resulting in strictly better robustness-accuracy trade-
 1052 offs (i.e., before certified accuracy started decreasing with lower α values). We trained a series of
 1053 potential teachers for CC-Dist with varying ℓ_1 coefficient and number of training epochs, and selected
 1054 the teacher depending on the performance of the resulting CC-Dist model. On all datasets except
 1055 TinyImageNet, where longer schedules were beneficial to CC-Dist performance, we found a teacher
 1056 trained with the relatively short 30-epoch schedule to result in strong CC-Dist performance. Finally,
 1057 generally speaking, we advocate for the re-use of the selected CC-IBP α coefficient for CC-Dist.
 1058 On TinyImageNet, the only setting where the employed α values for the reported models differ
 1059 across CC-Dist and CC-IBP, we found a larger CC-Dist α to result in simultaneously better standard
 1060 performance and certified robustness compared to all results from the literature. Nevertheless, re-using
 1061 $\alpha = 3 \times 10^{-3}$ for CC-Dist produced a model with 44.08% standard accuracy and 27.40% certified
 1062 accuracy (compare with table 1), which, albeit not improving on both metrics at once compared to
 1063 the MTL-IBP results from (Mao et al., 2025), significantly improves upon the overall performance
 1064 trade-offs seen in the literature.

1065 Unless otherwise stated, all hyper-parameters throughout the experimental evaluations comply with
 1066 those reported in table 3.

1066 D.3 VERIFICATION SETUP

1067 The employed verification setup is analogous to the one from De Palma et al. (2024b). As stated
 1068 in §5, we use the open source OVAL verification framework (Bunel et al., 2018; 2020a; De Palma
 1069 et al., 2021), which performs branch-and-bound, and a configuration based on alpha-beta-CROWN
 1070 bounds (Wang et al., 2021). Before running branch-and-bound, we try verifying the property via
 1071 IBP and CROWN bounds from `auto_LiRPA` (Xu et al., 2020), or to falsify it through a PGD
 1072 attack (Madry et al., 2018). Differently from De Palma et al. (2024b), we use a timeout of 600
 1073 seconds (as opposed to 1800 seconds). We perform verification by running the framework to compute
 1074 $\min_i \mathbf{z}_{f_\theta}^{C_\epsilon}(\mathbf{x}, y)_i$, where the min operator is converted into an equivalent auxiliary ReLU network to
 1075 append to $\mathbf{z}_{f_\theta}(\mathbf{x}, y)$ (Bunel et al., 2020b; De Palma et al., 2024b). For TinyImageNet and downscaled
 1076 ImageNet, differently from De Palma et al. (2024b), in order to reduce the size of the auxiliary
 1077 network, we exclude from the min operator all the logit differences that were already proved to
 1078 be positive by the IBP or CROWN bounds computed before running branch-and-bound. Finally,
 1079 the configuration employed to verify the TinyImageNet and downscaled ImageNet teacher models

(results reported in table 2) computes looser pre-activation bounds (using CROWN (Zhang et al., 2018) as opposed to 5 iterations of alpha-CROWN (Xu et al., 2021)) at the root of branch-and-bound: this was found to be a more effective verifier for networks trained via pure adversarial training.

D.4 SOFTWARE ACKNOWLEDGMENTS AND LICENSES

As described above, our code relies on the OVAL verification framework to verify the models, which was released under an MIT license. The training codebase is analogous to the one from the expressive losses work (De Palma et al., 2024b), also released under an MIT license: this was in turn based on the codebase from Shi et al. (2021), released under a 3-Clause BSD license. Both above repositories, and hence our codebase, rely on the `auto_LiRPA` (Xu et al., 2020) framework for incomplete verification, which has a 3-Clause BSD license. Concerning datasets: downscaled ImageNet was obtained from the ImageNet website (<https://www.image-net.org/download.php>), and TinyImageNet from the website of the CS231n Stanford class (<http://cs231n.stanford.edu/TinyImageNet-200.zip>). MNIST and CIFAR-10 were instead downloaded using `torchvision.datasets` (Paszke et al., 2019).

E SUPPLEMENTARY EXPERIMENTS

This appendix reports experimental results omitted from the main paper.

E.1 EFFECT OF DISTILLATION

Aiming to shed further light behind the effect of knowledge distillation in this context, we here present a more detailed experimental comparison between the CC-IBP and CC-Dist models from table 1, presenting [AutoAttack \(Croce & Hein, 2020\)](#) accuracy to measure empirical robustness, and the IBP loss to measure the ease of verifiability. As we can conclude from table 4, the use of knowledge distillation improves trade-offs between standard accuracy and certified robustness by:

1. transferring some of the superior natural accuracy and empirical robustness of the teacher onto the student through the distillation term;
2. preserving a large degree of verifiability through the CC-IBP term within the CC-Dist loss.

Table 4: Detailed analysis of the effect on distillation onto CC-IBP.

Dataset	ϵ	Method	Standard acc. [%]	AA acc. [%]	Certified acc. [%]	IBP loss
CIFAR-10	$\frac{2}{255}$	CC-DIST	81.55	70.71	64.60	29.05
		CC-IBP	79.51	68.56	63.50	27.46
	$\frac{8}{255}$	CC-DIST	55.13	36.80	35.52	1.865
		CC-IBP	54.46	36.59	35.42	1.862
TinyImageNet	$\frac{1}{255}$	CC-DIST	43.78	32.30	27.88	59.63
		CC-IBP	41.28	30.12	26.53	39.39
ImageNet64	$\frac{1}{255}$	CC-DIST	28.17	17.87	13.96	50.46
		CC-IBP	25.94	16.51	13.69	30.66

E.2 OTHER SPECIAL CASES OF THE PROPOSED DISTILLATION LOSS

As seen in proposition 3.2, when choosing $\alpha \in [0, 1]$, the proposed distillation loss ${}^{CC}\mathcal{R}_{f_\theta}^{C_\epsilon}(\alpha; \mathbf{x}, y)$ can continuously interpolate between lower and upper bounds to the worst-case feature-space distillation loss in equation (8). While §3.3 advocates for the use of the same α coefficient employed by CC-IBP in order to closely mirror its loss (see lemma 3.3), we expect other choices of the α coefficient to work well on selected benchmarks. We here evaluate the behavior of two training schemes that correspond to other special cases of the proposed parametrized distillation loss. Specifically, we consider the use of ${}^{CC}\mathcal{R}_{f_\theta}^{C_\epsilon}(0; \mathbf{x}, y) = \mathcal{R}_{f_\theta}^{C_\epsilon}(\mathbf{x}, y)$ and ${}^{CC}\mathcal{R}_{f_\theta}^{C_\epsilon}(1; \mathbf{x}, y) = \bar{\mathcal{R}}_{f_\theta}^{C_\epsilon}(\mathbf{x}, y)$ on top of CC-IBP,

1134 calling the resulting training schemes CC-Dist₀ and CC-Dist₁, respectively:

$$\begin{aligned} 1135 \quad \mathcal{L}^{\text{CC-Dist}^0}(\alpha, \beta; \mathbf{x}, y) &:= {}^{\text{CC}}\mathcal{L}_{f_\theta}^{\mathcal{C}_\epsilon}(\alpha; \mathbf{x}, y) + \beta {}^{\text{CC}}\mathcal{R}_{f_\theta}^{\mathcal{C}_\epsilon}(0; \mathbf{x}, y), \\ 1136 \quad \mathcal{L}^{\text{CC-Dist}^1}(\alpha, \beta; \mathbf{x}, y) &:= {}^{\text{CC}}\mathcal{L}_{f_\theta}^{\mathcal{C}_\epsilon}(\alpha; \mathbf{x}, y) + \beta {}^{\text{CC}}\mathcal{R}_{f_\theta}^{\mathcal{C}_\epsilon}(1; \mathbf{x}, y). \\ 1137 \end{aligned}$$

1138 Keeping ℓ_1 regularization and the α coefficient of the CC-IBP loss fixed, we first tested different distillation coefficients β while using the teachers employed for the CC-Dist models (see tables 2 and 3), finding that $\beta = 5/w$ yields the largest natural accuracy improvement for both methods on $\epsilon = 8/255$, and a strong trade-off between certified robustness and standard performance for CC-Dist₀ on $\epsilon = 2/255$. We found $\beta = (5 \times 10^{-4})/w$ to work better for CC-Dist₁ on $\epsilon = 2/255$. Then, using the above distillation coefficients, and similarly to what done for CC-Dist (see appendix D.2.4), we tested the two methods using teachers with varying ℓ_1 regularization and trained for 30 epochs. Aiming to compare them with CC-Dist, Table 5 reports results for the best-performing CC-Dist₀ and CC-Dist₁ models from the above procedure that display similar performance profiles with CC-Dist.

1139 Table 5 shows that both CC-Dist₀ and CC-Dist₁ work well across the considered CIFAR-10 settings. As we would expect considering the low employed α coefficient (see table 3), CC-Dist₀ strictly 1140 outperforms CC-Dist₁ on $\epsilon = 2/255$, where both methods nevertheless improve on both the standard 1141 performance and the certified accuracy of CC-IBP. While CC-Dist₀ displays performance comparable 1142 to CC-Dist in this setting, CC-Dist₁ performs markedly worse. On $\epsilon = 8/255$, where the employed α 1143 coefficient is instead relatively large (see table 3), CC-Dist₁ strictly outperforms CC-Dist₀ on both 1144 reported performance profiles, indicating the benefit of distilling onto feature IBP bounds in this 1145 context. Nevertheless, both methods can produce models improving on CC-IBP for both metrics on 1146 $\epsilon = 8/255$, with the corresponding CC-Dist₀ model strictly outperformed by CC-Dist.

1147 We believe that the above results further confirm the effectiveness of using empirically-robust models 1148 to improve certified training via knowledge distillation. As the relative performance of CC-Dist₀ 1149 and CC-Dist₁ varies depending on the experimental setting, we advocate for the use of CC-Dist as 1150 described in §3.3 due to its adaptive nature. Nevertheless, given that most considered benchmarks 1151 require relatively low α coefficients (see table 3), we expect CC-Dist₀ to be a valid alternative to 1152 CC-Dist on TinyImageNet and downscaled ImageNet.

1153

1154 E.3 DISTILLATION ONTO OTHER CERTIFIED TRAINING SCHEMES

1155

1156 In order to showcase the wider applicability of knowledge distillation from empirically-robust teachers, we here present results on applying such distillation process onto other certified training schemes, 1157 focusing on SABR (Müller et al., 2023), MTL-IBP (De Palma et al., 2024b), and IBP-R (De Palma 1158 et al., 2022). While the first two algorithms are expressive losses (De Palma et al., 2024b) like 1159 CC-IBP, which is the focus of this paper, IBP-R does not fit into the relative framework. As described 1160 in §4, SABR computes IBP bounds over a subset of \mathcal{C}_ϵ , termed a “small box”. We propose to employ 1161 a distillation loss of the form of ${}^{\text{CC}}\mathcal{R}_{f_\theta}^{\mathcal{C}_\epsilon}(1; \mathbf{x}, y)$, yet using IBP bounds computed on the small box, 1162 calling the resulting algorithm SABR-Dist. For MTL-IBP, which takes convex combinations between 1163 $\mathcal{L}_{f_\theta}^{\mathcal{C}_\epsilon}(\mathbf{x}, y)$ and $\bar{\mathcal{L}}_{f_\theta}^{\mathcal{C}_\epsilon}(\mathbf{x}, y)$, we employ the same distillation loss used for CC-Dist: ${}^{\text{CC}}\mathcal{R}_{f_\theta}^{\mathcal{C}_\epsilon}(1; \mathbf{x}, y)$.

1164

1165 Table 5: Comparison between the CC-Dist models from table 1 and other special cases of the proposed 1166 parametrized distillation loss.

1167

1168	Dataset	ϵ	Method	β	Teacher ℓ_1	Standard acc. [%]	Certified acc. [%]
1169		$\frac{2}{255}$	CC-DIST	$5/w$	10^{-5}	81.55	64.60
			CC-DIST ₀	$5/w$	10^{-5}	81.74	64.22
			CC-DIST ₁	$(5 \times 10^{-4})/w$	5×10^{-5}	79.84	63.93
1170	CIFAR-10		CC-IBP	0	/	79.51	63.50
			CC-DIST	$5/w$	5×10^{-6}	55.13	35.52
			CC-DIST ₀	$5/w$	2×10^{-5}	55.63	35.08
		$\frac{8}{255}$	CC-DIST ₁	$5/w$	2×10^{-6}	55.91	35.35
			CC-DIST ₀	$2/w$	5×10^{-6}	54.65	35.46
			CC-DIST ₁	$2/w$	5×10^{-6}	54.87	35.55
			CC-IBP	0	/	54.46	35.42

Table 6: Effect of distillation from empirically-robust teachers onto SABR (Müller et al., 2023), **MTL-IBP** (De Palma et al., 2024b), and **IBP-R** (De Palma et al., 2022).

Dataset	ϵ	Method	Std. acc. [%]	PGD-40 acc. [%]	Cert. acc. [%]
CIFAR-10	$\frac{2}{255}$	SABR-Dist	81.18	71.13	64.54
		SABR	79.55	69.49	63.94
	$\frac{2}{255}$	MTL-IBP-Dist	81.58	71.88	64.09
		MTL-IBP	79.71	69.67	63.16
	$\frac{8}{255}$	IBP-R-Dist	81.13	70.28	61.76
		IBP-R	79.68	69.98	61.43

Similarly to CC-Dist, and in spite of the lack of the coupling provided by lemma 3.2, we re-use the same α coefficient as for MTL-IBP. We note, nevertheless, that, for any given α , the MTL-IBP loss upper bounds the CC-IBP loss (De Palma et al., 2024b, proposition 4.2). For IBP-R, we instead use ${}^{CC}\mathcal{R}_{f_\theta}^{C_\epsilon}(0; \mathbf{x}, y)$ as distillation loss (see appendix E.2). Various teachers and distillation coefficients were tested for IBP-R, whereas we only varied β and kept the same teacher as table 2 for SABR and MTL-IBP. $\beta = 5/w$ was chosen for all methods. For IBP-R a teacher with ℓ_1 coefficient of 2×10^{-5} was selected. Table 6 shows that the distillation process successfully improves both the standard accuracy and the certified robustness of **all the three considered methods**, demonstrating the wider potential of distillation from adversarially-trained teachers towards certified training.

E.4 LOGIT-BASED DISTILLATION

We now compare the results of our proposed distillation loss from §3.2 with a loss that instead seeks to directly distill onto the CC-IBP convex combinations ${}^{CC}\mathbf{z}_{f_\theta}^{C_\epsilon}(\alpha; \mathbf{x}, y)$. Specifically, it employs a KL term between ${}^{CC}\mathbf{z}_{f_\theta}^{C_\epsilon}(\alpha; \mathbf{x}, y)$ and the teacher logit differences $\mathbf{z}_{t_{\theta^t}}(\mathbf{x}, y)$, resulting in the following training loss:

$${}^{CC}\mathcal{L}_{f_\theta}^{C_\epsilon}(\alpha; \mathbf{x}, y) + T^2 \beta \text{KL}_T \left(-{}^{CC}\mathbf{z}_{f_\theta}^{C_\epsilon}(\alpha; \mathbf{x}, y), -\mathbf{z}_{t_{\theta^t}}(\mathbf{x}, y) \right). \quad (15)$$

Keeping all other hyper-parameters fixed (including the teacher model) to the values reported in table 3, we tested different distillation coefficients β , using $T = 20$. We found that, compared to CC-IBP, the best performance profile using equation (15) were obtained using $\beta = (10^4)/w$ for both considered CIFAR-10 setups, whose results are reported in table 7. CC-Dist outperforms the logit-space distillation loss in both settings. We ascribe this to the more informative content of the model features, and to the inherent difference between the training goals of the teacher and the student, which are respectively trained for empirical and certified adversarial robustness. Allowing the student to learn a markedly different classification head from the teacher may be beneficial in this context.

E.5 PREACTRESNET18 TEACHERS

We now present a preliminary evaluation of the effect of employing a PreActResNet18 (PRN18) architecture (He et al., 2016) as teacher for CC-Dist. In order to ensure that the feature space of the teacher is set to the output of a ReLU, in compliance with the student model, we place the PreActResNet18 average pooling layer before the last ReLU and batch normalization (the standard PreActResNet18 architecture places it instead before the last linear layer). Focusing on TinyImageNet, and keeping $\alpha = 3 \times 10^{-3}$ and the ℓ_1 coefficient to 5×10^{-5} as for the CC-IBP model on this setup (see table 3), we tested various PRN18 teachers trained for 30 epochs with varying ℓ_1 regularization as CC-Dist teachers. Table 8 compares the performance of the ensuing CC-Dist model having the

Table 7: Comparison between the logit-space distillation from equation (15) and the CC-Dist models from table 1.

Dataset	ϵ	Method	Standard acc. [%]	Certified acc. [%]
CIFAR-10	$\frac{2}{255}$	CC-DIST	81.55	64.60
		EQ. (15)	80.61	63.65
CIFAR-10	$\frac{8}{255}$	CC-DIST	55.13	35.52
		EQ. (15)	54.76	35.20

1242 Table 8: Evaluation of the effect of PreActResNet18 (PRN18) teachers (tch.) on the TinyImageNet performance
 1243 of CC-Dist, compared to teachers with the same architecture as the student.

Dataset	ϵ	Tch. arch.	Std. acc. [%]	Cert. acc. [%]	Tch. std. acc. [%]	Tch. PGD-40 acc. [%]
TinyImageNet	$\frac{1}{255}$	CNN-7	44.08	27.40	47.18	36.07
		PRN18	43.03	26.09	50.90	39.98

1244
 1245
 1246
 1247
 1248
 1249
 1250 largest natural accuracy with the best model obtained through same-architecture teachers for these
 1251 hyper-parameters, and the respective teachers. CC-Dist draws no benefit from the PRN18 teacher
 1252 (which was trained with ℓ_1 coefficient equal to 5×10^{-5}), in spite of the fact that it displays stronger
 1253 performance than the CNN-7 teacher. While we are hopeful that better CC-Dist results could be
 1254 obtained by training PRN18 teachers for longer (the considered teachers are trained for 30 epochs, as
 1255 opposed to the 100 epochs employed for the CNN-7 teacher), we leave this for future work.
 1256

1257 E.6 EXPERIMENTAL VARIABILITY

1258
 1259 Owing to the large cost of repeatedly training and verifying certifiably-robust models (the worst-case
 1260 per-image verification runtime is 600 seconds: see appendices D.1 and D.3), and as common in the
 1261 area (De Palma et al., 2024b; Mao et al., 2023; Müller et al., 2023; Mao et al., 2024a; 2025), all the
 1262 experiments were run using a single seed. In order to provide an indication of experimental variability,
 1263 table 9 presents aggregated CIFAR-10 results over 4 repetitions for CC-Dist and CC-IBP. These
 1264 include the CC-Dist and CC-IBP results reported in table 1 and 3 further repetitions of the associated
 1265 experiment, consisting of training and the ensuing verification using branch-and-bound. We found
 1266 experimental variability to be relatively low on $\epsilon = 2/255$, and more noticeable on $\epsilon = 8/255$. On
 1267 the latter setting, distillation markedly improves the average standard accuracy while leaving certified
 1268 robustness roughly unvaried. For $\epsilon = 2/255$, CC-Dist instead produces a significant improvement
 1269 on both average metrics at once. In both cases, the cumulative (signed) improvement across the two
 1270 averaged metrics is similar to the one reported in table 1.

1271 E.7 RUNTIME MEASUREMENTS

1272
 1273 In order to assess the training overhead associated with our distillation scheme, we here present
 1274 runtime measurements and estimates for CC-Dist and CC-IBP. Specifically, we provide the training
 1275 runtime of both methods, separately including also the teacher training runtime for CC-Dist, and
 1276 estimates of the verification runtimes for the trained models from table 1. These experiments were
 1277 carried out using an Nvidia RTX 8000 GPU, and 6 cores of an AMD EPIC 7302 CPU. Table 10
 1278 shows that, under the training schedules of appendix D.2.2 and when training teachers for 30 epochs
 1279 as per table D.2.4, CC-Dist is associated with minimal training overhead on the considered CIFAR-10
 1280 settings. This overhead increases to respectively almost 70% and 40% for TinyImageNet and down-
 1281 scaled ImageNet, where stronger teachers are required in order to maximize performance. Finally, the
 1282 increased certified accuracy of the CC-Dist models (see table 1) comes with an increased verification
 1283 runtime, as expected from the increases IBP loss resulting from the distillation process (see table 4).
 1284
 1285

1286 Table 9: Experimental variability of CC-Dist and CC-IBP on CIFAR-10: maximal and minimal values, the mean
 1287 and its standard error (SEM) across 4 repetitions are reported.

Dataset	ϵ	Method	Standard acc. [%]				Certified acc. [%]			
			Mean	SEM	Max	Min	Mean	SEM	Max	Min
CIFAR-10	$\frac{2}{255}$	CC-DIST	81.58	0.08	81.72	81.38	64.46	0.14	64.61	64.03
		CC-IBP	79.68	0.08	79.90	79.51	63.41	0.10	63.65	63.21
	$\frac{8}{255}$	CC-DIST	55.22	0.07	55.40	55.09	34.88	0.24	35.52	34.40
		CC-IBP	54.12	0.19	54.62	53.73	34.89	0.23	35.42	34.34

1296 Table 10: Training runtime measurements for CC-Dist, their respective teachers (trained for 30 epochs), and
 1297 CC-IBP under the training schedules of appendix D.2.2.

1298	Dataset	ϵ	Method	Training runtime [s]	Teacher training runtime [s]	Estimated [†] verification runtime [s]
1300	CIFAR-10	$\frac{2}{255}$	CC-DIST	1.605×10^4	2.225×10^3	1.097×10^5
1301			CC-IBP	1.568×10^4	/	7.089×10^4
1302		$\frac{8}{255}$	CC-DIST	1.653×10^4	2.223×10^3	1.090×10^4
1303			CC-IBP	1.600×10^4	/	6.238×10^3
1304	TinyImageNet	$\frac{1}{255}$	CC-DIST	5.432×10^4	3.470×10^4	2.778×10^5
1305			CC-IBP	5.246×10^4	/	1.608×10^5
1306	ImageNet64	$\frac{1}{255}$	CC-DIST	3.228×10^5	1.089×10^5	1.210×10^6
1307			CC-IBP	3.095×10^5	/	7.794×10^5

1308 [†]Extrapolated from measurements over the first 500 test images.

1310 E.8 DIFFERENT ARCHITECTURE AND ACTIVATION FUNCTION

1312 The main results focus on the CNN-7 architecture owing to its state-of-the-art performance and
 1313 prevalence in the relevant literature (De Palma et al., 2024b; Mao et al., 2023; Müller et al., 2023; Shi
 1314 et al., 2021). We here investigate whether the distillation process is beneficial beyond this context by
 1315 studying the relative performance of CC-Dist on a different activation function and on a different
 1316 architecture for both the teacher and the model, focussing on CIFAR-10 with $\epsilon = 2/255$. For the
 1317 activation experiment, we modify CNN-7 to employ the hyperbolic tangent (tanh), testing different
 1318 teachers trained for 100 epochs (choosing a teacher ℓ_1 coefficient of 2×10^{-5}), and varying β values
 1319 (settling for $\beta = 5/w$ as for the experiments in table 1). For the architecture experiment, we use
 1320 PreActResNet18 (PRN18) for both the teacher and the student, testing different teachers trained for
 1321 30 epochs (settling on a teacher with ℓ_1 coefficient of 5×10^{-6}), and using $\beta = 5/w$. In both cases,
 1322 owing to the lack of support for either model from the OVAL branch-and-bound framework (Bunel
 1323 et al., 2018; 2020a; De Palma et al., 2021) employed throughout the paper, we use CROWN (Zhang
 1324 et al., 2018) from auto_LiRPA (Xu et al., 2020) as post-training verification algorithm. Table 11
 1325 shows that CC-Dist successfully improves robustness-accuracy trade-offs for both the considered
 1326 settings, demonstrating the wider applicability of the proposed distillation technique.

1327 E.9 DISTILLATION ON EARLIER LATENTS

1329 Throughout the paper, we define the feature space as the activations before last affine network layer,
 1330 in accordance with the conditions of lemma 3.2. We here investigate the effect of computing on the
 1331 distillation loss $CC\mathcal{R}_{f_\theta}^{C_\epsilon}(\alpha; \mathbf{x}, y)$ on an earlier feature space, corresponding to the activations before
 1332 the penultimate affine layer of CNN-7. In particular, we focus on CIFAR-10 with $\epsilon = 2/255$, keeping
 1333 the teacher model fixed to the one used for tables 1 and 2 and varying the β coefficient to account for
 1334 the change in the feature space: we found $\beta = 2/w$ to yield the maximize performance in this context.
 1335 Table 12 shows that distillation for the last affine layer yields strictly better robustness-accuracy
 1336 trade-offs than those presented in table 5.1. As distilling on earlier layers implies that a larger
 1337 portion of the network is exclusively trained using the CC-IBP loss, we ascribe this to insufficient
 1338 teacher-student coupling.

1339 E.10 CLEAN TEACHERS

1341 In spite of our focus on learning from adversarially-trained teachers, the proposed distillation loss
 1342 $CC\mathcal{R}_{f_\theta}^{C_\epsilon}(\alpha; \mathbf{x}, y)$ only makes use of the clean features of the teacher model. In order to investigate
 1343

1344 Table 11: Effect of distillation beyond CNN-7 students on CIFAR-10 with $\epsilon = 2/255$.

1345 (a) Modified CNN-7 with tanh activation functions.

1346	Method	Std. acc. [%]	CROWN acc. [%]
1347	CC-Dist	72.38	49.42
1348	CC-IBP	71.29	47.39

1346 (b) PreActResNet18 architecture.

1347	Method	Std. acc. [%]	CROWN acc. [%]
1348	CC-Dist	74.01	53.63
1349	CC-IBP	73.40	52.88

1350
1351 Table 12: Effect of computing the distillation loss ${}^{CC}\mathcal{R}_{f_\theta}^{\mathcal{C}_\epsilon}(\alpha; \mathbf{x}, y)$ on an earlier feature space.
1352
1353
1354

Dataset	ϵ	Feature space	Std. acc. [%]	Cert. acc. [%]
CIFAR-10	$\frac{2}{255}$	Last	81.55	64.60
		Penultimate	80.84	63.11

1355
1356 whether the empirical robustness of the teacher is indeed necessary for an effective distillation process,
1357 we here study the effect of employing standard-trained teachers. In particular, focusing on CIFAR-10
1358 with $\epsilon = 2/255$, we keep $\beta = 2/w$ and test the use of SGD-trained teachers trained with varying ℓ_1
1359 regularization coefficients (5×10^{-6} being the chosen ℓ_1 coefficient). Table 13 shows that the use of
1360 standard teachers markedly worsens the certified accuracy of the student, which is now inferior to the
1361 one associated to CC-IBP (see table 1). These results demonstrate that a robust teacher representation
1362 is a key requirement for the success of the distillation process.
1363
1364

1365 F DETAILS ON THE EMPLOYED NOTATION

1366 We here provide additional details on the employed notation.
1367

1368 **Student and teacher models** Input-to-logits maps are denoted using the letter f , defined as the
1369 composition of a feature map, denoted using the letter h , and classification heads, denoted using the
1370 letter g . We employ a subscript to denote the parameters of these (sub-)networks, here written as a
1371 function of their inputs only. Network parameters, denoted θ throughout this work, are subscripted
1372 to denote the subsets of θ corresponding to the feature map θ_h , and to the classification head, θ_g ,
1373 respectively. The (sub-)networks for the teacher model, and their parameters, are denoted by the use
1374 of the t superscript (e.g., θ_h^t or $h_{\theta_h^t}^t$).
1375

1376 **Bounds to worst-case quantities** The worst-case classification loss, equation (3), and the worst-
1377 case distillation loss, equation (8), are superscripted by the relative local perturbation set \mathcal{C}_ϵ around
1378 the input \mathbf{x} . Lower and upper bounds to both quantities are denoted through lower and upper bars,
1379 respectively (e.g., $\mathcal{L}_{f_\theta}^{\mathcal{C}_\epsilon}(\mathbf{x}, y)$), with the superscript preserved to stress their local validity. A similar
1380 notation is employed for the local bounds to the worst-case logit differences (e.g., $\mathbf{z}_{f_\theta}^{\mathcal{C}_\epsilon}(\mathbf{x}, y)$), which
1381 lower bounds equation 2. Convex combinations between lower and upper bounds, parametrized
1382 by α , are denoted by left-superscript CC standing for Convex Combination (e.g., ${}^{CC}\mathcal{R}_{f_\theta}^{\mathcal{C}_\epsilon}(\alpha; \mathbf{x}, y)$),
1383 without any bars. For all these worst-case quantities, lower bounds corresponding to evaluations on
1384 concrete inputs from adversarial attacks, and the upper bounds are obtained through network convex
1385 relaxations (specifically, IBP).
1386

1387 **Bounds to the student features** We again employ a similar notation when bounding the student
1388 features $h_{\theta_h}(\mathbf{x})$, defined in proposition 3.1. In this context, both the lower and the upper bounds are
1389 obtained through IBP. Convex combinations between the adversarial student latents $h_{\theta_h}(\mathbf{x}_{\text{adv}})$ and
1390 the IBP lower and upper bounds, as defined in equation 9, are denoted by the left-superscript CC and
1391 lower and upper bars, respectively (e.g., ${}^{CC}\bar{h}_{\theta_h}^{\mathcal{C}_\epsilon}(\alpha; \mathbf{x})$).
1392

1393
1394 Table 13: Effect of performing distillation from clean teachers.
1395
1396
1397
1398
1399

Dataset	ϵ	Teacher training	Std. acc. [%]	Cert. acc. [%]
CIFAR-10	$\frac{2}{255}$	PGD-10 Standard	81.55 81.48	64.60 62.52